INVERSE PROBLEMS IN SCIENCE AND ENGINEERING, 2017
http://dx.doi.org/10.1080/17415977.2016.1273919

Taylor & Francis
Taylor & Francis Group

A numerical reconstruction method in inverse elastic scattering

F. S. V. Bazán[a], J. B. Francisco[a], K. H. Leem[b], G. Pelekanos[a] and V. Sevroglou[c]

[a]Department of Mathematics, Federal University of Santa Catarina, Florianopolis, Brazil; [b]Department of Mathematics and Statistics, Southern Illinois University, Edwardsville, IL, USA; [c]Department of Statistics and Insurance Science, University of Piraeus, Piraeus, Greece

ABSTRACT

In this paper a new numerical method for the shape reconstruction of obstacles in elastic scattering is proposed. Initially, the direct scattering problem for a rigid body and the mathematical setting for the corresponding inverse one are presented. Inverse uniqueness issues for the general case of mixed boundary conditions on the boundary of our obstacle, which are valid for a rigid body as well are established. The inversion algorithm based on the factorization method is presented into a suitable form and a new numerical scheme for the reconstruction of the shape of the scatterer, using far-field measurements, is given. In particular, an efficient Tikhonov parameter choice technique, called *Improved Maximum Product Criterion* (IMPC) and its linchpin within the framework of the factorization method is exploited. Our regularization parameter is computed via a fast iterative algorithm which requires no *a priori* knowledge of the noise level in the far-field data. Finally, the effectiveness of IMPC is illustrated with various numerical examples involving a kite, an acorn, and a peanut-shaped object.

ARTICLE HISTORY
Received 3 October 2016
Accepted 15 December 2016

KEYWORDS
Inverse elastic scattering problems; reciprocity gap functional (RGF); factorization method; improved maximum product criterion (IMPC)

AMS SUBJECT CLASSIFICATIONS
74B05; 35P25; 45A05; 65F22

1. Introduction

A lot of work has been done for direct scattering problems as well as for inverse ones. The latter problems require the determination of the physical and/or geometrical properties of the elastic obstacle, from a knowledge of the asymptotic behaviour of the scattered field, the so-called far-field pattern.

In this work the inverse elastic scattering problem of shape reconstruction of scattering objects will be studied. Emphasis on the numerical treatment of the above problem, using far-field pattern of the scattered wave, will be given. In particular, our aim is to extend the combination of the well-known *factorization method* [1,2], originally developed in the acoustic context by Colton and Kirsch [3], and an improved version of the *maximum product criterion* (MPC) developed by Bazán et al. [4] to the more complicated elastic scattering case. In particular, we will provide reconstructions of two-dimensional rigid bodies irradiated by incident elastic plane waves. The main idea of the method is that the support of the scattering obstacle is obtained by solving a vector integral equation of

CONTACT bsevro@unipi.gr

the first kind and noting that a specific norm becomes unbounded as a point lying on a rectangular grid containing the scatterer approaches its boundary.

Factorization method (the so-called $(F^{\star}F)^{1/4}$-method), is well known to yield an ill posed far-field equation customarily solved via Tikhonov regularization with the regularization parameter computed via Morozov's discrepancy principle [5]. However, Morozov's discrepancy principle requires the computation of the zeros of the discrepancy function at each point of the grid, a process that is time-consuming. Moreover, the noise level in the data should be known *a priori*, something that in real-life applications is not the case in general. In order to avoid these problems, we employ a variant of the MPC, the so-called Improved Maximum Product Criterion (IMPC), which computes regularized solution norms and corresponding residual norms, and chooses as regularization parameter the critical point associated with the largest local maximum of the product of these norms as a function of the regularization parameter. In addition, as with MPC, IMPC does not depend on user specified input parameters (like subspace dimension or truncating parameter) and requires no *a priori* knowledge of the noise level. As we mentioned before, IMPC extends in a very elegant way the maximum product criterion, and it has been applied with great success in reconstructing three-dimensional obstacles in acoustics [6] and in electromagnetic scattering applications [7].

We organize our paper as follows. In Section 2, the direct scattering problem for a rigid body irradiated by an incident elastic plane wave is considered. The corresponding inverse elastic scattering problem, taking into account the general case of mixed boundary conditions, which covers the Dirichlet case (rigid body) as well, is also presented. Further, uniqueness results are established, based on a mixed reciprocity relation using incident plane waves as well as point-sources. In Section 3, the *factorization method* is considered and its linchpin with the inversion scheme is presented. Finally, in Section 4 a numerical technique called IMPC will be presented. Using IMPC, the regularization parameter will be computed via a fast iterative algorithm which requires no *a priori* knowledge of the noise level in the data. Various numerical results concerning the reconstruction of a kite, an acorn and a peanut-shaped object are given, showing the applicability of the method.

2. Formulation of the problem

2.1. The direct scattering problem

We formulate our problem by considering the scattering process of a given time-harmonic elastic plane wave $\widetilde{\mathbf{u}}^{\text{inc}}$ by an impenetrable obstacle $D \subset \mathbb{R}^2$ which is open, bounded and simply connected domain. Its smooth boundary ∂D is of class C^2, and we assume that $\mathbb{R}^2$ is filled up with a homogeneous and isotropic elastic medium with Lamé constant coefficients μ, λ and mass density ρ. We assume the strong elliptic conditions

$$\mu > 0, \quad 2\mu + \lambda > 0. \tag{1}$$

We denote by $\hat{\mathbf{n}}_r$ the outward unit normal vector on the boundary ∂D almost everywhere at point $\mathbf{r}$, and the complement of our scatterer D, will be referred as the exterior domain, denoted by $\mathbb{R}^2 \setminus \overline{D}$. The total displacement elastic field $\widetilde{\mathbf{u}}$ is viewed as the sum of the incident

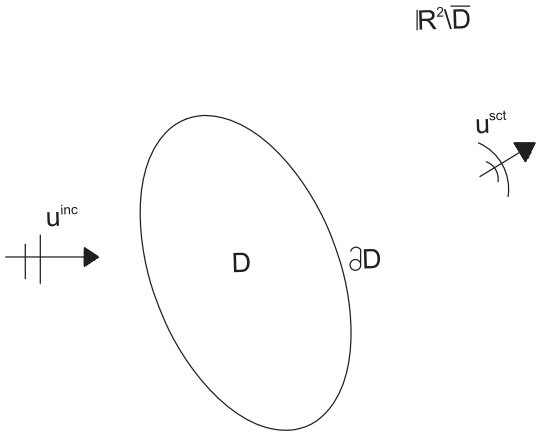

Figure 1. The elastic rigid scatterer *D*.

field $\widetilde{\mathbf{u}}^{\text{inc}}$ and the scattered field $\widetilde{\mathbf{u}}^{sct}$, i.e.

$$\widetilde{\mathbf{u}}(\mathbf{r}) = \widetilde{\mathbf{u}}^{\text{inc}}(\mathbf{r}) + \widetilde{\mathbf{u}}^{\text{sct}}(\mathbf{r}), \quad \mathbf{r} \in \mathbb{R}^2 \setminus \overline{\mathrm{D}}, \tag{2}$$

where $\widetilde{\mathbf{u}}^{\text{inc}}$ is the dyadic elastic plane wave of the form

$$\widetilde{\mathbf{u}}^{\text{inc}}(\mathbf{r}) = \hat{\mathbf{d}} \otimes \hat{\mathbf{d}}\, \mathrm{e}^{\mathrm{i}k_{\mathrm{p}}\mathbf{r}\cdot\hat{\mathrm{d}}} + (\widetilde{\mathrm{I}} - \hat{\mathbf{d}} \otimes \hat{\mathbf{d}})\, \mathrm{e}^{\mathrm{i}k_{\mathrm{s}}\mathbf{r}\cdot\hat{\mathrm{d}}}, \tag{3}$$

where k_p is the longitudinal wave number, k_s the transverse one, $\widetilde{\mathrm{I}}$ is the 2×2 identity matrix, $\hat{\mathbf{d}} = (\cos\theta,\ \sin\theta)$ the direction of propagation,

$$\widetilde{\mathrm{I}} - \hat{\mathbf{d}} \otimes \hat{\mathbf{d}} = \hat{\mathbf{d}}^{\perp} \otimes \hat{\mathbf{d}}^{\perp} \tag{4}$$

with $\hat{\mathbf{d}}^{\perp}$ being the polarization vector and $\hat{\mathbf{d}} \in \mathrm{S}_1 := \{\hat{\mathbf{d}} \in \mathbb{R}^2 : |\ \hat{\mathbf{d}}\ | = 1\}$. At this point, we mention that our scatterer could also be irradiated only by an incident plane P-wave (longitudinal wave) given by the first term of the right-hand side of (3), i.e.

$$\widetilde{\mathbf{u}}_{\mathrm{p}}^{\text{inc}}(\mathbf{r}) = \hat{\mathbf{d}} \otimes \hat{\mathbf{d}}\, \mathrm{e}^{\mathrm{i}k_{\mathrm{p}}\mathbf{r}\cdot\hat{d}}, \tag{5}$$

or, only by a plane S-wave (transverse wave) given by the second term of the right-hand side of (3) of the form

$$\widetilde{\mathbf{u}}_{\mathrm{s}}^{\text{inc}}(\mathbf{r}) = (\widetilde{\mathrm{I}} - \hat{\mathbf{d}} \otimes \hat{\mathbf{d}})\, \mathrm{e}^{\mathrm{i}k_{\mathrm{s}}\mathbf{r}\cdot\hat{\mathrm{d}}} \tag{6}$$

(recall this later in the numerical examples, see Section 4). In relations (2)–(6) the '$\sim$' sign denote dyadic fields. We use this notation for two reasons: the first one is due to the dyadic nature of the free-space Green's function of the Navier equation. The second one arises from the fact that dyadic's symmetry formulation for a scattering problem is higher than the corresponding vector formulation [8], and therefore the propagation vector alone suffices to specify the incident field. As an excellent source of reference concerning properties of dyads we give the book by Tai [9].

We now state the direct scattering problem which is described by the following boundary value problem: For a given incident dyadic elastic plane wave $\widetilde{\mathbf{u}}^{\text{inc}}$, find the total elastic

field $\widetilde{\mathbf{u}} \in \left[C^2(\mathbb{R}^2 \setminus \overline{D})\right]^2 \cap \left[C^1(\mathbb{R}^2 \setminus D)\right]^2$, such that

$$\mu\, \Delta\widetilde{\mathbf{u}}(\mathbf{r}) + (\lambda + \mu)\, \nabla\nabla \cdot \widetilde{\mathbf{u}}(\mathbf{r}) + \rho\, \omega^2\, \widetilde{\mathbf{u}}(\mathbf{r}) = \widetilde{\mathbf{0}}, \quad \mathbf{r} \in \mathbb{R}^2 \setminus \overline{D} \tag{7}$$

$$\widetilde{\mathbf{u}}(\mathbf{r}) = \widetilde{\mathbf{0}}, \quad \mathbf{r} \in \partial D \tag{8}$$

$$\lim_{\mathrm{r}\to\infty} \sqrt{\mathrm{r}} \left(\frac{\partial \widetilde{\mathbf{u}}_\beta^{\mathrm{sct}}(\mathbf{r})}{\partial \mathrm{r}} - \mathrm{i}\mathrm{k}_\beta\, \widetilde{\mathbf{u}}_\beta^{\mathrm{sct}}(\mathbf{r}) \right) = \widetilde{\mathbf{0}}, \quad \beta = \mathrm{p}, \mathrm{s}, \quad \mathrm{r} := |\mathbf{r}|, \tag{9}$$

where $\omega \in \mathbb{R}_+$ is the frequency. Relation (8) is the Dirichlet boundary condition which corresponds to a body whose surface cannot be deformed by the stresses generated by the incident displacement field. Such a body is called *rigid scatterer* and the scattering configuration is shown in Figure 1. The Sommerfeld-Kupradze type radiation conditions (9) [10,11] holds uniformly in all directions $\hat{\mathbf{r}} = \mathbf{r}/r$ for both P and S-components of the scattered field $\widetilde{\mathbf{u}}_p^{\mathrm{sct}}$, $\widetilde{\mathbf{u}}_s^{\mathrm{sct}}$, respectively. In addition, the well-known Helmholtz decomposition for the displacement field holds and is expressed as [10]:

$$\widetilde{\mathbf{u}}(\mathbf{r}) = \widetilde{\mathbf{u}}_{\mathrm{p}}(\mathbf{r}) + \widetilde{\mathbf{u}}_{\mathrm{s}}(\mathbf{r}) \;\text{ with }\; (\Delta + \mathrm{k}_{\mathrm{p}}^2)\, \widetilde{\mathbf{u}}_{\mathrm{p}}(\mathbf{r}) = \widetilde{\mathbf{0}}, \quad (\Delta + \mathrm{k}_{\mathrm{s}}^2)\, \widetilde{\mathbf{u}}_{\mathrm{s}}(\mathbf{r}) = \widetilde{\mathbf{0}}, \tag{10}$$

$$\mathrm{k}_{\mathrm{p}} = \omega \sqrt{\frac{\rho}{2\mu + \lambda}}, \quad k_s = \omega \sqrt{\frac{\rho}{\mu}}, \tag{11}$$

where $\widetilde{\mathbf{u}}_{\mathrm{p}}(\mathbf{r})$ is the longitudinal part (P-wave being rotational-free), $\widetilde{\mathbf{u}}_{\mathrm{s}}(\mathbf{r})$ the transverse part (S-wave divergence-free) and k_{p}, k_{s} are the corresponding wave numbers (see also relations (3), (5) and (6)).

From now on, and in order to write equation (7) in an abbreviation form, we employ the notation for the differential operator Δ^*:

$$\Delta^* = \mu\, \Delta + (\lambda + \mu)\, \nabla\nabla\cdot, \tag{12}$$

with Δ being the Laplace operator. In addition, we will also need the stress operator T on the boundary ∂D defined as follows:

$$\mathrm{T}^{(\mathbf{r})} = 2\mu\, \hat{\mathbf{n}}_{\mathrm{r}} \cdot \nabla\, + \lambda\, \hat{\mathbf{n}}_{\mathrm{r}} \nabla \cdot\, + \mu\, \hat{\mathbf{n}}_{\mathrm{r}} \times \nabla\times, \tag{13}$$

where '$\cdot$' and '$\times$' denote the scalar and the vector product, respectively. The superscript in (13) denotes the action of the differential operator on the indicated variable and will be omitted from now on.

Remark 2.1: The above direct scattering problem (7)–(9) can be reformulated in integral form, following either the direct method, based on Betti's formulae [10], or the indirect method using single and double layer potentials. Solvability issues can be treated with analogous arguments (boundary integral equation approach) as those used in [12] and [11]. Our aim in the work at hand is the study of the corresponding inverse elastic problem, and therefore, we do not present these solvability results for the sake of brevity.

In what follows, we now present the free-space Green's dyadic $\widetilde{\Gamma}(\mathbf{r}, \mathbf{r}')$ of the Navier equation (7). It satisfies the following equation

$$\Delta^* \widetilde{\Gamma}(\mathbf{r}, \mathbf{r}') + \rho\, \omega^2\, \widetilde{\Gamma}(\mathbf{r}, \mathbf{r}') = -\widetilde{\mathrm{I}}\, \delta(\mathbf{r} - \mathbf{r}'), \quad \mathbf{r}, \mathbf{r}' \in \mathbb{R}^2 \tag{14}$$

with $\delta(\mathbf{r}-\mathbf{r}')$ being the Dirac measure concentrated at the point $\mathbf{r}$, and is given, [13], by

$$\widetilde{\Gamma}(\mathbf{r},\,\mathbf{r}') = \frac{\mathrm{i}}{4}\left\{\frac{1}{\mu}\,\widetilde{\mathrm{I}}\,\mathrm{H}_0^{(1)}(\mathrm{k_s}|\mathbf{r}-\mathbf{r}'|) - \frac{1}{\rho\,\omega^2}\,\nabla_{\mathbf{r}}\otimes\nabla_{\mathbf{r}}\left[H_0^{(1)}(\mathrm{k_p}|\mathbf{r}-\mathbf{r}'|) - \mathrm{H}_0^{(1)}(\mathrm{k_s}|\mathbf{r}-\mathbf{r}'|)\right]\right\}, \tag{15}$$

where $\mathrm{H}_0^{(1)}(\cdot)$ is the cylindrical Hankel function of the first kind and zero order, and '$\otimes$' is the juxtaposition between two vectors which gives a dyadic.

From the numerical point of view (see later Section 4), we want to avoid the dyadic nature of the fundamental solution. Hence, if $\mathbf{p}\in\mathrm{S}_1$ denotes the polarization of an elastic point-source at any $\mathbf{y}_\mathrm{o}\in\mathbb{R}^2$, then $\mathbf{u}(\mathbf{r}) = \widetilde{\Gamma}(\mathbf{r},\,\mathbf{y}_\mathrm{o})\cdot\mathbf{p}$. In what follows, we will adopt the notation $\widetilde{\Gamma}(\mathbf{r},\,\mathbf{y}_\mathrm{o})\cdot\mathbf{p}\equiv\boldsymbol{\Gamma}(\mathbf{r},\,\mathbf{y}_\mathrm{o};\,\mathbf{p})$, $\mathbf{r}\in\mathbb{R}^2\setminus\{\mathbf{y}_\mathrm{o}\}$. For the dyadic approach for elastic scattering problems we refer to [14] and the references therein.

Using asymptotic analysis for $\boldsymbol{\Gamma}(\mathbf{r},\,\mathbf{y}_\mathrm{o};\,\mathbf{p})$ we can arrive at

$$\boldsymbol{\Gamma}(\mathbf{r},\,\mathbf{y}_\mathrm{o};\,\mathbf{p}) = \Gamma^{\infty,\mathrm{p}}(\hat{\mathbf{r}},\,\mathbf{y}_\mathrm{o};\,\mathbf{p})\,\hat{\mathbf{r}}\,\frac{\mathrm{e}^{\mathrm{ik_p r}}}{\sqrt{\mathrm{r}}} + \Gamma^{\infty,\mathrm{s}}(\hat{\mathbf{r}},\,\mathbf{y}_\mathrm{o};\,\mathbf{p})\,\hat{\mathbf{r}}^{\perp}\,\frac{\mathrm{e}^{\mathrm{ik_s r}}}{\sqrt{\mathrm{r}}} + \mathrm{O}(\mathrm{r}^{-3/2}),\quad \mathrm{r}\to\infty \tag{16}$$

with $\hat{\mathbf{r}}^{\perp}$ being the perpendicular vector to $\hat{\mathbf{r}}$. In the latter case, the far-field patterns

$$\boldsymbol{\Gamma}^{\infty}(\cdot,\,\mathbf{y}_\mathrm{o};\,\mathbf{p}) = (\Gamma^{\infty,\mathrm{p}}(\cdot,\,\mathbf{y}_\mathrm{o};\,\mathbf{p}),\,\Gamma^{\infty,\mathrm{s}}(\cdot,\,\mathbf{y}_\mathrm{o};\,\mathbf{p})) \tag{17}$$

of this elastic point source of the P and S-part of $\Gamma(\mathbf{r},\,\mathbf{y}_\mathrm{o};\,\mathbf{p})$ are given by [13]

$$\Gamma^{\infty,\mathrm{p}}(\hat{\mathbf{r}},\,\mathbf{y}_\mathrm{o};\,\mathbf{p}) = \frac{1}{\lambda+2\mu}\,\frac{\mathrm{i}+1}{4\sqrt{\pi\,\mathrm{k_p}}}\,\mathrm{e}^{-\mathrm{ik_p}\hat{\mathbf{r}}\cdot\mathbf{y}_\mathrm{o}}\,\hat{\mathbf{r}}\cdot\mathbf{p}, \tag{18}$$

$$\Gamma^{\infty,\mathrm{s}}(\hat{\mathbf{r}},\,\mathbf{y}_\mathrm{o};\,\mathbf{p}) = \frac{1}{\mu}\,\frac{\mathrm{i}+1}{4\sqrt{\pi\,k_s}}\,\mathrm{e}^{-\mathrm{ik_s}\hat{\mathbf{r}}\cdot\mathbf{y}_\mathrm{o}}\,\hat{\mathbf{r}}^{\perp}\cdot\mathbf{p}, \tag{19}$$

respectively. In addition, the surface traction (see (13)) of the fundamental solution for $\mathbf{r}\in\Omega_\mathrm{R} = \{\mathbf{d}\in\mathbb{R}^2:\ |\mathbf{d}| = \mathrm{R}\}$ can be computed, and after some calculations we can get the following asymptotic formula [15]

$$\mathrm{T}\,\boldsymbol{\Gamma}(\mathbf{r},\,\mathbf{y}_\mathrm{o};\,\mathbf{p}) = \mathrm{T}\,\Gamma^{\infty,\mathrm{p}}(\hat{\mathbf{r}},\,\mathbf{y}_\mathrm{o};\,\mathbf{p})\,\hat{\mathbf{r}}\,\frac{\mathrm{e}^{\mathrm{ik_p r}}}{\sqrt{\mathrm{r}}} + \mathrm{T}\,\Gamma^{\infty,\mathrm{s}}(\hat{\mathbf{r}},\,\mathbf{y}_\mathrm{o};\,\mathbf{p})\,\hat{\mathbf{r}}^{\perp}\,\frac{\mathrm{e}^{\mathrm{ik_s r}}}{\sqrt{\mathrm{r}}} + \mathrm{O}(\mathrm{r}^{-3/2}),\quad \mathrm{r}\to\infty \tag{20}$$

where

$$\mathrm{T}\,\Gamma^{\infty,\mathrm{p}}(\hat{\mathbf{r}},\,\mathbf{y}_\mathrm{o};\,\mathbf{p}) = \frac{\mathrm{i}-1}{4}\sqrt{\frac{\mathrm{k_p}}{\pi}}\,\mathrm{e}^{-\mathrm{ik_p}\hat{\mathbf{r}}\cdot\mathbf{y}_\mathrm{o}}\,\hat{\mathbf{r}}\cdot\mathbf{p}, \tag{21}$$

$$\mathrm{T}\,\Gamma^{\infty,\mathrm{s}}(\hat{\mathbf{r}},\,\mathbf{y}_\mathrm{o};\,\mathbf{p}) = \frac{\mathrm{i}-1}{4}\sqrt{\frac{\mathrm{k_s}}{\pi}}\,\mathrm{e}^{-\mathrm{ik_s}\hat{\mathbf{r}}\cdot\mathbf{y}_\mathrm{o}}\,\hat{\mathbf{r}}^{\perp}\cdot\mathbf{p}. \tag{22}$$

We also want to obtain the asymptotic form of the radiating solution $\widetilde{\mathbf{u}}^{\mathrm{sct}}$ of the Navier equation (7). Exploiting Betti's formulae, through asymptotic analysis and taking into account (16) and (18)–(22), we arrive at

$$\widetilde{\mathbf{u}}^{\mathrm{sct}}(\mathbf{r}) = \widetilde{\mathbf{u}}^{\infty,\mathrm{p}}\,\frac{\mathrm{e}^{\mathrm{i}k_{\mathrm{p}}\mathrm{r}}}{\sqrt{\mathrm{r}}} + \widetilde{\mathbf{u}}^{\infty,\mathrm{s}}(\hat{\mathbf{r}})\,\frac{\mathrm{e}^{\mathrm{i}k_{\mathrm{s}}\mathrm{r}}}{\sqrt{\mathrm{r}}} + \mathrm{O}(\mathrm{r}^{-3/2}), \tag{23}$$

uniformly with respect to $\hat{\mathbf{r}} = \mathbf{r}/\mathrm{r}$ and $\mathrm{r} = |\mathbf{r}| \to \infty$. The functions $\widetilde{\mathbf{u}}^{\infty,\mathrm{p}}$ and $\widetilde{\mathbf{u}}^{\infty,\mathrm{s}}$ (coefficients of the terms $\mathrm{e}^{\mathrm{i}k_\beta \mathrm{r}}/\sqrt{\mathrm{r}}$, $\beta = \mathrm{p}, \mathrm{s}$) are the corresponding far-field patterns, defined on the unit circle in $\mathbb{R}^2$, and are known as the longitudinal and the transverse far-field patterns, respectively. The latter functions are also analytic functions and are considered as elements of $L^2(\Omega)$. From the point of view of the investigation of the inverse scattering problem, the far-field patterns, which consists a measure of the scattered field at the radiation zone, are essential and useful on the numerical reconstructions of obstacles. Various formulas and expressions for elastic far-field patterns can be found in [16,17] and [18].

In what follows we deal with the corresponding inverse elastic scattering problem of (7)–(9). In particular, the inverse problem consists *in the determination of the unknown boundary ∂D of the rigid scatterer D, from the knowledge of the far-field pattern of the scattered field*. For such an inverse problem, a modification of the factorization method is needed, and an inversion algorithm combined with a new numerical reconstruction method for rigid bodies will be presented.

2.2. Inverse scattering problem: the general case of mixed boundary conditions

In this subsection we will establish the unique determination of an elastic scatterer D (rigid obstacle) using the far-field pattern for all incident waves. Our methodology is based on an essential mixed reciprocity relation. From the point of view of applications, we will focus on the more general case. i.e. the case of having mixed boundary conditions on the boundary ∂D of our obstacle. We consider that our simply connected boundary is consisted by two parts, a Dirichlet (rigid) one and a Robin (impedance) one. On the Dirichlet part of ∂D the displacement is given, whereas on the impedance part, a specific combination physically expressing the proportionality relation between the displacement and its surface stress, is given. Obstacles characterized by boundary conditions of this type are often called *partially coated* (see [12, p.184]) and there is a lot of study and active research on inverse problems for elastic, acoustic and electromagnetic media. Partially coated obstacles have various applications on elastic materials and are very extensive. In particular, we give the following examples: (a) Cases of high temperatures concerning non destructive tests for coating imperfections due to thermal shock [19]. (b) Cases of non destructive evaluation which use elastic waves for the measurement of elastic properties in solid specimens [20]. (c) Cases of engineering mechanics in medicine, see, e.g. [21] a stent coated with a drug which is constructed to control the release of the drug into surrounding tissue. This process has the property to slow down the growth of unwanted cells and gives the opportunity the blood vessel to heal. We also mention that we can find a lot of other applications concerning partially coated obstacles, such as in materials science, in civil and mechanical engineering, in nanomechanics [22,23], etc.

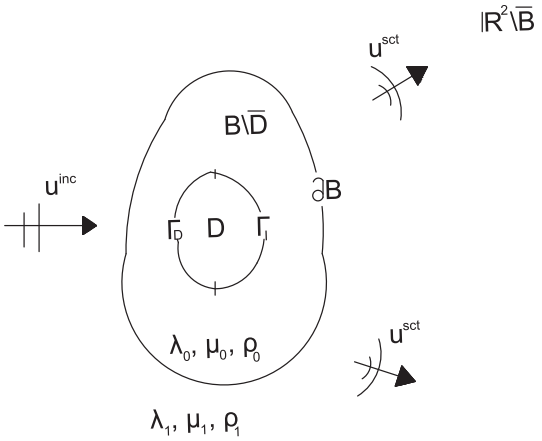

Figure 2. The partially coated obstacle D. The case $\Gamma_I = \emptyset$ corresponds to the rigid scatterer.

We continue our study by considering the boundary ∂D consisting of two parts, the so-called Dirichlet part Γ_D and the impedance part Γ_I such that $\partial D \equiv \Gamma = \overline{\Gamma}_D \cup \overline{\Gamma}_I$, where Γ_D, Γ_I are two disjoint, relatively open subsets of the boundary Γ. We can also consider that our scatterer D is embedded in a piecewise-constant background medium $B \subset \mathbb{R}^2$ with a C^2-boundary ∂B.

Therefore, we next deal with the inverse elastic scattering problem concerning a mixed partially coated obstacle embedded in a piecewise homogeneous background medium. It is described by the following mixed impedance transmission boundary value problem: *Determine uniquely the partially coated obstacle D and its physical properties if the following conditions hold*

$$\Delta^*\widetilde{\mathbf{u}}(\mathbf{r}) + \rho_0\,\omega^2\,\widetilde{\mathbf{u}}(\mathbf{r}) = \widetilde{\mathbf{0}} \quad \text{in } \mathbb{R}^2 \setminus \overline{B}, \tag{24}$$

$$\Delta^*\widetilde{\mathbf{u}}(\mathbf{r}) + \rho_1\,\omega^2\,\widetilde{\mathbf{u}}(\mathbf{r}) = \widetilde{\mathbf{0}} \quad \text{in B} \setminus \overline{D}, \tag{25}$$

$$\widetilde{\mathbf{u}}(\mathbf{r}) = \widetilde{\mathbf{0}} \quad \text{on } \Gamma_D, \tag{26}$$

$$\mathrm{T}\widetilde{\mathbf{u}}(\mathbf{r}) + i\,\omega\,\mathrm{c}\,\widetilde{\mathbf{u}}(\mathbf{r}) = \widetilde{\mathbf{0}} \quad \text{on } \Gamma_I, \tag{27}$$

$$\lim_{\mathrm{r}\to\infty} \sqrt{r}\left(\frac{\partial \widetilde{\mathbf{u}}_\beta^{\mathrm{sct}}(\mathbf{r})}{\partial r} - \mathrm{i}k_\beta\,\widetilde{\mathbf{u}}_\beta^{\mathrm{sct}}(\mathbf{r})\right) = \widetilde{\mathbf{0}}, \quad \beta = \mathrm{p,s}, \tag{28}$$

where $\widetilde{\mathbf{u}}(\mathbf{r}) = \widetilde{\mathbf{u}}^{\mathrm{inc}}(\mathbf{r}) + \widetilde{\mathbf{u}}^{\mathrm{sct}}(\mathbf{r})$ in $(\mathbb{R}^2 \setminus \overline{B}) \cup (B \setminus \overline{D})$. Relation (27) is the impedance (Robin type) boundary condition in the field of elasticity. The part Γ_I of the boundary in Figure 2, is due to a coating on the Robin part of the boundary with a material of surface impedance. Such a surface with finite impedance has an intermediate behaviour between the rigid surface and the cavity (stress-free surface) [24]. Impedance expresses (intensity × stiffness) in relation to wave diffraction, reflection, etc. and measures the contrast between two media. The notion for impedance in elasticity is discussed with details in [25]. Throughout this paper c (the surface impedance for the boundary Γ_I) will be considered a positive constant and $\omega \in \mathbb{R}_+$ is the frequency. We also assume that on the discontinuity interface ∂B, we have to consider transmission conditions, requiring the continuity of the displacement

and stress vector across ∂B, i.e.

$$\widetilde{\mathbf{u}}^{\text{ext}} = \widetilde{\mathbf{u}}^{\text{int}}, \qquad \mathrm{T}_e\,\widetilde{\mathbf{u}}^{\text{ext}} = \mathrm{T}_i\,\widetilde{\mathbf{u}}^{\text{int}} \qquad \text{on } \partial B \tag{29}$$

where $\widetilde{\mathbf{u}}^{int}$, $\widetilde{\mathbf{u}}^{\text{ext}}$ denote the interior and exterior one sides limits (traces) on the interface ∂B, respectively, and the notations $\mathrm{T_i}\,\widetilde{\mathbf{u}}^{int}$, $\mathrm{T_e}\,\widetilde{\mathbf{u}}^{\text{ext}}$ are given by relation (13), if we replace the Lamé constants $\lambda,\ \mu$ with the appropriate values $\lambda_{\mathrm{j}},\ \mu_{\mathrm{j}},\ \mathrm{j} = 0$ or 1. The above piecewise-constant functions, λ_{j} and μ_{j} are the Lamé constants, ρ_{j} are the densities of the elastic layers, satisfying the relations $\mu_{\mathrm{j}} > 0,\ \ 2\mu_{\mathrm{j}} + \lambda_{\mathrm{j}} > 0,\ \ \rho_{\mathrm{j}} > 0,\ \ \mathrm{j} = 0, 1$ with $\lambda_0,\ \mu_0$ and ρ_0 stand for the domain $\mathbb{R}^2 \setminus \overline{B}$, whereas $\lambda_1,\ \mu_1$ and ρ_1 for the domain $\mathrm{B} \setminus \overline{D}$. Further, the $\mathrm{k_{j,p}},\ \mathrm{k_{j,s}},\ \mathrm{j} = 0, 1$ (as before, see (11)), are the corresponding wave numbers for the longitudinal and the transverse waves, respectively, given by

$$\mathrm{k_{j,p}} = \omega\sqrt{\frac{\rho_{\mathrm{j}}}{\lambda_{\mathrm{j}} + 2\mu_{\mathrm{j}}}}, \quad \mathrm{k_{j,s}} = \omega\sqrt{\frac{\rho_{\mathrm{j}}}{\mu_{\mathrm{j}}}}, \quad \mathrm{j} = 0, 1. \tag{30}$$

In relation (28) we indicate that $\mathrm{k}_\beta = \mathrm{k}_{0,\beta},\ \beta = \mathrm{p}, \mathrm{s}$.

Concerning the direct scattering problem, corresponding to the inverse problem (24)–(28), its solvability has been proved via the potential method [26]. In particular, we reduced our problem to a system of pseudodiffential equations and established that the corresponding boundary integral operators are invertible in appropriate Bessel potential and Besov spaces [12]. In addition, regularity results were proved and the case of Lipschitz surfaces was also treated.

Remark 2.2: Relations (26) and (27) constitute the mixed impedance boundary conditions on the boundary Γ of the scatterer. The case $\Gamma_I = \emptyset$ (*Dirichlet case*) corresponds to an elastic *rigid body* (see boundary condition (8) and our following inverse uniqueness result (corresponding to the direct scattering problem (7)–(9)) is still valid as well.

In order to establish uniqueness we have to prove mixed reciprocity relation (see later relation (34)), which holds for a partially coated obstacle as well as for a rigid body. Its worthmentioning here, that the derivation of mixed scattering relations are essential for the *point-source method* [27].

We will establish such a relation relating plane wave incidence to point-source incidence. Therefore, we need to consider incident-plane-waves as well as point-sources, and for the reader's convenience we recall the following notation: For incident plane waves

$$\widetilde{\mathbf{u}}^{\text{tot}}(\mathbf{r}; \hat{\mathbf{d}}) = \widetilde{\mathbf{u}}^{\text{inc}}(\mathbf{r}; \hat{\mathbf{d}}) + \widetilde{\mathbf{u}}^{\text{sct}}(\mathbf{r}; \hat{\mathbf{d}}), \tag{31}$$

whereas, for point-sources

$$\widetilde{\mathbf{u}}^{\text{tot}}_{\mathbf{y}_o}(\mathbf{r}) = \widetilde{\mathbf{u}}^{\text{inc}}_{\mathbf{y}_o}(\mathbf{r}) + \widetilde{\mathbf{u}}^{\text{sct}}_{\mathbf{y}_o}(\mathbf{r}), \tag{32}$$

with $\hat{\mathbf{d}} \in \mathrm{S}_1$ and $\mathbf{y}_o \in \mathbb{R}^2$ the point-source. We recall that our incident point-source field is given by $\widetilde{\mathbf{u}}^{\text{inc}}_{\mathbf{y}_o}(\mathbf{r}) := \widetilde{\Gamma}(\mathbf{r},\, \mathbf{y}_o),\ \mathbf{r} \neq \mathbf{y}_o$ (this is actually similar to the fundamental solution (15)) and that $\widetilde{\mathbf{u}}_\infty(\hat{\mathbf{r}}; \hat{d})$ and $\widetilde{\mathbf{u}}_{\infty,\mathbf{y}_o}(\hat{\mathbf{r}})$ are the far-field patterns of $\widetilde{\mathbf{u}}^{\text{sct}}(\mathbf{r}; \hat{\mathbf{d}})$ and $\widetilde{\mathbf{u}}^{\text{sct}}_{\mathbf{y}_o}(\mathbf{r})$, respectively.

The proof of the following result is based on a special functional form, the so-called **Elastic Reciprocity Gap Functional** (**RGF**) defined as [15]:

$$\mathbf{RGF}(\widetilde{\mathbf{u}},\widetilde{\mathbf{v}}) = [\,\widetilde{\mathbf{u}},\,\widetilde{\mathbf{v}}\,]_{\partial B} := \int_{\partial \mathrm{B}} \Big[\,(\mathrm{T}\,\widetilde{v}(\mathbf{r}))^{\top}\cdot\widetilde{u}(\mathbf{r}) - \widetilde{v}(\mathbf{r})^{\top}\cdot\mathrm{T}\,\widetilde{u}(\mathbf{r})\,\Big]\,\mathrm{d}s(\mathbf{r}) \tag{33}$$

which is also employed in the study of various inverse problems, see, [15,28,29].

We are now ready to prove the following theorem.

Theorem 2.3: *For the scattering of an incident point-source wave field* $\widetilde{\mathbf{u}}^{inc}_{\mathbf{y}_0}(\mathbf{r}) := \widetilde{\Gamma}(\mathbf{r},\,\mathbf{y}_{\mathrm{o}})$ *and an incident plane wave* $\widetilde{\mathbf{u}}^{inc}(\mathbf{r};\,-\hat{\mathbf{b}})$ *propagating in the direction* $-\hat{\mathbf{b}}$*, by a rigid obstacle D, the following relation holds:*

$$\widetilde{\mathbf{u}}_{\infty,\mathrm{y_o}}(\hat{\mathbf{b}}) = \Big(\widetilde{\mathbf{u}}^{sct}(\mathbf{y}_{\mathrm{o}},-\hat{\mathbf{b}})\Big)^{\top}, \qquad \mathbf{y}_{\mathrm{o}}\in\mathbf{R}^2\setminus\overline{B}. \tag{34}$$

***Proof*:** Let $\mathbf{y}_{\mathrm{o}}\in\mathbb{R}^2\setminus\overline{B}$. Using relations (31), (32) and the bilinearity of (33) we can easily arrive at

$$[\widetilde{\mathbf{u}}^{\mathrm{t}}_{\mathrm{y_o}}(\mathbf{r}),\ \widetilde{\mathbf{u}}^{\mathrm{t}}(\mathbf{r};\,-\hat{\mathbf{b}})]_{\partial B} = [\widetilde{\mathbf{u}}^{\mathrm{inc}}_{\mathrm{y_o}}(\mathbf{r}),\,\widetilde{\mathbf{u}}^{\mathrm{t}}(\mathbf{r};\,-\hat{\mathbf{b}})]_{\partial B} + [\widetilde{\mathbf{u}}^{\mathrm{sct}}_{\mathrm{y_o}}(\mathbf{r}),\,\widetilde{\mathbf{u}}^{\mathrm{t}}(\mathbf{r};\,-\hat{\mathbf{b}})]_{\partial B}. \tag{35}$$

We now have to calculate the two surface integrals $[\widetilde{\mathbf{u}}^{\mathrm{sct}}_{\mathrm{y_o}}(\mathbf{r}),\,\widetilde{\mathbf{u}}^{t}(\mathbf{r};\,-\hat{\mathbf{b}})]_{\partial B}$ and $[\widetilde{\mathbf{u}}^{\mathrm{inc}}_{\mathrm{y_o}}(\mathbf{r}),\,\widetilde{\mathbf{u}}^{t}(\mathbf{r};\,-\hat{\mathbf{b}})]_{\partial B}$. Via Betti's formulae, the Sommerfeld−Kupradze radiation condition and the integral representation of the far-field pattern $\widetilde{\mathbf{u}}_{\infty,\,\mathrm{y_o}}(\hat{\mathbf{b}})$, we have that

$$\widetilde{\mathbf{u}}_{\infty,\,\mathrm{y_o}}(\hat{\mathbf{b}}) = [\widetilde{\mathbf{u}}^{\mathrm{sct}}_{\mathrm{y_o}}(\mathbf{r}),\,\widetilde{\mathbf{u}}^{t}(\mathbf{r};\,-\hat{\mathbf{b}})]_{\partial \mathrm{B}}, \tag{36}$$

or, equivalently

$$\widetilde{\mathbf{u}}_{\infty,\,\mathrm{y_o}}(\hat{\mathbf{b}}) = \int_{\partial \mathrm{B}}\Big[\Big(\mathrm{T}\,\widetilde{\mathbf{u}}^{t}(\mathbf{r};\,-\hat{\mathbf{b}})\Big)^{\top}\cdot\widetilde{\mathbf{u}}^{\mathrm{sct}}_{\mathrm{y_o}}(\mathbf{r}) - \Big(\widetilde{\mathbf{u}}^{t}(\mathbf{r};\,-\hat{\mathbf{b}})\Big)^{\top}\cdot\mathrm{T}\,\widetilde{\mathbf{u}}^{\mathrm{sct}}_{\mathrm{y_o}}(\mathbf{r})\Big]\,\mathrm{ds}(\mathbf{r}). \tag{37}$$

With the aid of (32) and the boundary conditions (29) on ∂B, the latter can be written as

$$\begin{aligned}
&\widetilde{\mathbf{u}}_{\infty,\,\mathrm{y_o}}(\hat{\mathbf{b}})\\
&= \int_{\partial \mathrm{B}}\Big[\Big(\mathrm{T}\,\widetilde{\mathbf{u}}^{t}(\mathbf{r};\,-\hat{\mathbf{b}})\Big)^{\top}\cdot\widetilde{\mathbf{u}}^{t}_{\mathrm{y_o}}(\mathbf{r}) - \Big(\widetilde{\mathbf{u}}^{t}(\mathbf{r};\,-\hat{\mathbf{b}})\Big)^{\top}\cdot\mathrm{T}\,\widetilde{\mathbf{u}}^{t}_{\mathrm{y_o}}(\mathbf{r})\Big]\,\mathrm{ds}(\mathbf{r})\\
&\quad -\int_{\partial \mathrm{B}}\Big[\Big(\mathrm{T}\,\widetilde{\mathbf{u}}^{t}(\mathbf{r};\,-\hat{\mathbf{b}})\Big)^{\top}\cdot\widetilde{\mathbf{u}}^{\mathrm{inc}}_{\mathrm{y_o}}(\mathbf{r}) - \Big(\widetilde{\mathbf{u}}^{t}(\mathbf{r};\,-\hat{\mathbf{b}})\Big)^{\top}\cdot\mathrm{T}\,\widetilde{\mathbf{u}}^{\mathrm{inc}}_{\mathrm{y_o}}(\mathbf{r})\Big]\,\mathrm{ds}(\mathbf{r}).
\end{aligned} \tag{38}$$

Taking now into account second Betti's formula, relation (38) yields

$$
\begin{aligned}
&\widetilde{\mathbf{u}}_{\infty,\,\mathrm{y_o}}(\hat{\mathbf{b}}) \\
&\quad= \int_{\Gamma}\left[\left(\mathrm{T}\,\widetilde{\mathbf{u}}^{\mathrm{t}}(\mathbf{r};-\hat{\mathbf{b}})\right)^{\top}\cdot\widetilde{\mathbf{u}}^{t}_{\mathrm{y_o}}(\mathbf{r})-\left(\widetilde{\mathbf{u}}^{\mathrm{t}}(\mathbf{r};-\hat{\mathbf{b}})\right)^{\top}\cdot\mathrm{T}\,\widetilde{\mathbf{u}}^{t}_{\mathrm{y_o}}(\mathbf{r})\right]\mathrm{ds}(\mathbf{r}) \\
&\qquad+\int_{\mathrm{B}\setminus\overline{\mathrm{D}}}\left[\left(\Delta^{*}\,\widetilde{\mathbf{u}}^{\mathrm{t}}(\mathbf{r};-\hat{\mathbf{b}})\right)^{\top}\cdot\widetilde{\mathbf{u}}^{\mathrm{t}}_{\mathrm{y_o}}(\mathbf{r})-\left(\widetilde{\mathbf{u}}^{\mathrm{t}}(\mathbf{r};-\hat{\mathbf{b}})\right)^{\top}\cdot\Delta^{*}\,\widetilde{\mathbf{u}}^{\mathrm{t}}_{\mathrm{y_o}}(\mathbf{r})\right]\mathrm{d}\upsilon \\
&\qquad-\int_{\Gamma}\left[\left(\mathrm{T}\,\widetilde{\mathbf{u}}^{t}(\mathbf{r};-\hat{\mathbf{b}})\right)^{\top}\cdot\widetilde{\mathbf{u}}^{\mathrm{inc}}_{\mathrm{y_o}}(\mathbf{r})-\left(\widetilde{\mathbf{u}}^{t}(\mathbf{r};-\hat{\mathbf{b}})\right)^{\top}\cdot\mathrm{T}\,\widetilde{\mathbf{u}}^{\mathrm{inc}}_{\mathrm{y_o}}(\mathbf{r})\right]\mathrm{ds}(\mathbf{r}) \\
&\qquad-\int_{\mathrm{B}\setminus\overline{\mathrm{D}}}\left[\left(\Delta^{*}\,\widetilde{\mathbf{u}}^{t}(\mathbf{r};-\hat{\mathbf{b}})\right)^{\top}\cdot\widetilde{\mathbf{u}}^{\mathrm{inc}}_{\mathrm{y_o}}(\mathbf{r})-\left(\widetilde{\mathbf{u}}^{t}(\mathbf{r};-\hat{\mathbf{b}})\right)^{\top}\cdot\Delta^{*}\,\widetilde{\mathbf{u}}^{\mathrm{inc}}_{\mathrm{y_o}}(\mathbf{r})\right]\mathrm{d}\upsilon. \quad (39)
\end{aligned}
$$

Since $\widetilde{\mathbf{u}}^{t}(\mathbf{r};-\hat{\mathbf{b}})$ and $\widetilde{\mathbf{u}}^{t}_{\mathrm{y_o}}(\mathbf{r})$ are regular solutions of the Navier Equation (25) in $B\setminus\overline{D}$, Equation (39) yields

$$
\begin{aligned}
&\widetilde{\mathbf{u}}_{\infty,\,\mathrm{y_o}}(\hat{\mathbf{b}}) \\
&\quad=-\int_{\Gamma}\left[\left(\mathrm{T}\,\widetilde{\mathbf{u}}^{\mathrm{t}}(\mathbf{r};-\hat{\mathbf{b}})\right)^{\top}\cdot\widetilde{\mathbf{u}}^{\mathrm{inc}}_{\mathrm{y_o}}(\mathbf{r})-\left(\widetilde{\mathbf{u}}^{\mathrm{t}}(\mathbf{r};-\hat{\mathbf{b}})\right)^{\top}\cdot\mathrm{T}\,\widetilde{\mathbf{u}}^{\mathrm{inc}}_{\mathrm{y_o}}(\mathbf{r})\right]\mathrm{ds}(\mathbf{r}) \\
&\qquad+\int_{\mathrm{B}\setminus\overline{\mathrm{D}}}(\rho_1-\rho_0)\;\omega^{2}\left(\widetilde{\mathbf{u}}^{\mathrm{t}}(\mathbf{r};-\hat{\mathbf{b}})\right)^{\top}\cdot\widetilde{\mathbf{u}}^{\mathrm{inc}}_{\mathrm{y_o}}(\mathbf{r})\,\mathrm{d}\upsilon. \quad (40)
\end{aligned}
$$

Concerning the other surface integral $[\,\widetilde{\mathbf{u}}^{\mathrm{inc}}_{\mathrm{y_o}}(\mathbf{r}),\,\widetilde{\mathbf{u}}^{t}(\mathbf{r};\,-\hat{\mathbf{b}})]_{\partial\mathrm{B}}$, we have the following manipulation:

$$
\begin{aligned}
&[\widetilde{\mathbf{u}}^{\mathrm{inc}}_{\mathrm{y_o}}(\mathbf{r}),\,\widetilde{\mathbf{u}}^{\mathrm{t}}(\mathbf{r};\,-\hat{\mathbf{b}})]_{\partial\mathrm{B}} \\
&\quad=[\widetilde{\mathbf{u}}^{\mathrm{inc}}_{\mathrm{y_o}}(\mathbf{r}),\,\widetilde{\mathbf{u}}^{\mathrm{inc}}(\mathbf{r};\,-\hat{\mathbf{b}})]_{\partial B}+[\widetilde{\mathbf{u}}^{\mathrm{inc}}_{\mathrm{y_o}}(\mathbf{r}),\,\widetilde{\mathbf{u}}^{\mathrm{sct}}(\mathbf{r};\,-\hat{\mathbf{b}})]_{\partial\mathrm{B}} \\
&\quad=\int_{\partial\mathrm{B}}\left[\left(\mathrm{T}\,\widetilde{\mathbf{u}}^{\mathrm{inc}}(\mathbf{r};-\hat{\mathbf{b}})\right)^{\top}\cdot\widetilde{\mathbf{u}}^{\mathrm{inc}}_{\mathrm{y_o}}(\mathbf{r})-\left(\widetilde{\mathbf{u}}^{\mathrm{inc}}(\mathbf{r};-\hat{\mathbf{b}})\right)^{\top}\cdot\mathrm{T}\,\widetilde{\mathbf{u}}^{\mathrm{inc}}_{\mathrm{y_o}}(\mathbf{r})\right]\mathrm{ds}(\mathbf{r}) \\
&\qquad+\int_{\partial\mathrm{B}}\left[\left(\mathrm{T}\,\widetilde{\mathbf{u}}^{\mathrm{sct}}(\mathbf{r};-\hat{\mathbf{b}})\right)^{\top}\cdot\widetilde{\mathbf{u}}^{\mathrm{inc}}_{\mathrm{y_o}}(\mathbf{r})-\left(\widetilde{\mathbf{u}}^{\mathrm{sct}}(\mathbf{r};-\hat{\mathbf{b}})\right)^{\top}\cdot\mathrm{T}\,\widetilde{\mathbf{u}}^{\mathrm{inc}}_{\mathrm{y_o}}(\mathbf{r})\right]\mathrm{ds}(\mathbf{r}). \quad (41)
\end{aligned}
$$

Using now the exterior integral representation (recall $\mathbf{y_o}\in\mathbb{R}^2\setminus\overline{B}$) for the scattered filed $\widetilde{\mathbf{u}}^{\mathrm{sct}}(\mathbf{y_o};\,-\hat{\mathbf{b}})$, the latter yields

$$
\begin{aligned}
&-\left(\widetilde{\mathbf{u}}^{\mathrm{sct}}(\mathbf{y_o};\,-\hat{\mathbf{b}})\right)^{\top} \\
&\quad=\int_{\partial\mathrm{B}}\left[\left(\mathrm{T}\,\widetilde{\mathbf{u}}^{t}(\mathbf{r};-\hat{\mathbf{b}})\right)^{\top}\cdot\widetilde{\mathbf{u}}^{\mathrm{inc}}_{\mathrm{y_o}}(\mathbf{r})-\left(\widetilde{\mathbf{u}}^{t}(\mathbf{r};-\hat{\mathbf{b}})\right)^{\top}\cdot\mathrm{T}\,\widetilde{\mathbf{u}}^{\mathrm{inc}}_{\mathrm{y_o}}(\mathbf{r})\right]\mathrm{ds}(\mathbf{r}). \quad (42)
\end{aligned}
$$

With the aid now of the boundary conditions (29) on ∂B and the second Betti's formula, Equation (42) takes the form

$$\begin{aligned}\left(\widetilde{\mathbf{u}}^{\mathrm{sct}}(\mathbf{y_o};-\hat{\mathbf{b}})\right)^{\top}&=-\int_{\Gamma}\left[\left(\mathrm{T}\,\widetilde{\mathbf{u}}^{\mathrm{t}}(\mathbf{r};-\hat{\mathbf{b}})\right)^{\top}\cdot\widetilde{\mathbf{u}}^{\mathrm{inc}}_{\mathrm{y_o}}(\mathbf{r})-\left(\widetilde{\mathbf{u}}^{\mathrm{t}}(\mathbf{r};-\hat{\mathbf{b}})\right)^{\top}\cdot\mathrm{T}\,\widetilde{\mathbf{u}}^{\mathrm{inc}}_{\mathrm{y_o}}(\mathbf{r})\right]\mathrm{ds}(\mathbf{r})\\&\quad-\int_{\mathrm{B}\setminus\overline{\mathrm{D}}}\left[\left(\Delta^{*}\,\widetilde{\mathbf{u}}^{\mathrm{t}}(\mathbf{r};-\hat{\mathbf{b}})\right)^{\top}\cdot\widetilde{\mathbf{u}}^{\mathrm{inc}}_{\mathrm{y_o}}(\mathbf{r})-\left(\widetilde{\mathbf{u}}^{\mathrm{t}}(\mathbf{r};-\hat{\mathbf{b}})\right)^{\top}\cdot\Delta^{*}\,\widetilde{\mathbf{u}}^{\mathrm{inc}}_{\mathrm{y_o}}(\mathbf{r})\right]\mathrm{d}\upsilon.\end{aligned}\tag{43}$$

Since now $\widetilde{\mathbf{u}}^{t}(\mathbf{r};-\hat{\mathbf{b}})$ and $\widetilde{\mathbf{u}}^{\mathrm{inc}}_{\mathrm{y_o}}(\mathbf{r})$ are regular solutions of the Navier equation in $B\setminus\overline{D}$ and $\mathbb{R}^2\setminus\overline{B}$, respectively, (43) can be written as:

$$\begin{aligned}\left(\widetilde{\mathbf{u}}^{\mathrm{sct}}(\mathbf{y_o};-\hat{\mathbf{b}})\right)^{\top}&=-\int_{\Gamma}\left[\left(\mathrm{T}\,\widetilde{\mathbf{u}}^{\mathrm{t}}(\mathbf{r};-\hat{\mathbf{b}})\right)^{\top}\cdot\widetilde{\mathbf{u}}^{\mathrm{inc}}_{\mathrm{y_o}}(\mathbf{r})-\left(\widetilde{\mathbf{u}}^{\mathrm{t}}(\mathbf{r};-\hat{\mathbf{b}})\right)^{\top}\cdot\mathrm{T}\,\widetilde{\mathbf{u}}^{\mathrm{inc}}_{\mathrm{y_o}}(\mathbf{r})\right]\mathrm{ds}(\mathbf{r})\\&\quad+\int_{\mathrm{B}\setminus\overline{\mathrm{D}}}(\rho_1-\rho_0)\,\omega^2\left(\widetilde{\mathbf{u}}^{t}(\mathbf{r};-\hat{\mathbf{b}})\right)^{\top}\cdot\widetilde{\mathbf{u}}^{\mathrm{inc}}_{\mathrm{y_o}}(\mathbf{r})\,\mathrm{d}\upsilon.\end{aligned}\tag{44}$$

Combining relations (35), (40) and (44) the assertion of the theorem easily follows. □

Similar mixed reciprocity relations remain true for other boundary conditions of rigid obstacles as well as for penetrable scatterers. We mention that general mixed reciprocity relations between far-field patterns based on reciprocity relations for two point-source incidences in two and three-dimensional linear elasticity are established in [16,30], whereas a more straightforward proof for these mixed reciprocity relations has been established in [31] (see also the references therein).

Theorem 2.4: *Let D_1 and $\breve{D}_1$ be two subsets of B, and let $\mathcal{G}$ be the unbounded component of $\mathbb{R}^2\setminus\left(\overline{D}_1\cup\overline{\breve{D}}_1\right)$. Furthermore, let $\widetilde{\mathbf{u}}^{sct}(\mathbf{r},\hat{\mathbf{d}})$, $\widetilde{\breve{\mathbf{u}}}^{sct}(\mathbf{r},\hat{\mathbf{d}})$ be the scattered fields due to obstacles D_1 and $\breve{D}_1$ with corresponding far-field patterns $\widetilde{\mathbf{u}}_{\infty}(\hat{\mathbf{r}},\hat{d})$ and $\widetilde{\breve{\mathbf{u}}}_{\infty}(\hat{\mathbf{r}},\hat{d})$, respectively. Assume*

$$\widetilde{\mathbf{u}}_{\infty}(\hat{\mathbf{r}},\hat{d})=\widetilde{\breve{\mathbf{u}}}_{\infty}(\hat{\mathbf{r}},\hat{d}),\quad\forall\,\hat{\mathbf{r}},\hat{\mathbf{d}}\in S_1.\tag{45}$$

Let $\widetilde{\mathbf{u}}^{sct}_{\mathbf{y_o}}(\mathbf{r})$ denotes the unique solution of the mixed impedance transmission boundary value problem

$$\Delta^{*}\widetilde{\mathbf{u}}^{sct}(\mathbf{r})+\rho_0\,\omega^2\,\widetilde{\mathbf{u}}^{sct}(\mathbf{r})=\widetilde{\mathbf{0}}\qquad in\quad\mathbb{R}^2\setminus\overline{B}\tag{46}$$

$$\Delta^{*}\widetilde{\mathbf{u}}^{sct}(\mathbf{r})+\rho_1\,\omega^2\,\widetilde{\mathbf{u}}^{sct}(\mathbf{r})=(\rho_0-\rho_1)\,\omega^2\,\widetilde{\Gamma}(\mathbf{r},\mathbf{y_o})\qquad in\quad B\setminus\overline{D}\tag{47}$$

$$\widetilde{\mathbf{u}}^{sct}_{e}(\mathbf{r})=\widetilde{\mathbf{u}}^{sct}_{i}(\mathbf{r})\quad\mathrm{T}_e\,\widetilde{\mathbf{u}}^{sct}_{e}(\mathbf{r})=\mathrm{T}_i\,\widetilde{\mathbf{u}}^{ext}_{i}(\mathbf{r})\qquad on\ \partial B\tag{48}$$

$$\widetilde{\mathbf{u}}^{sct}(\mathbf{r})=-\widetilde{\Gamma}(\mathbf{r},\mathbf{y_o})\qquad on\ \Gamma_D\tag{49}$$

$$\mathrm{T}\,\widetilde{\mathbf{u}}^{sct}(\mathbf{r})+i\,\omega c\,\widetilde{\mathbf{u}}^{sct}(\mathbf{r})=-\mathrm{T}\,\widetilde{\Gamma}(\mathbf{r},\mathbf{y_o})-i\,\omega c\,\widetilde{\Gamma}(\mathbf{r},\mathbf{y_o})\qquad on\quad\Gamma_I\tag{50}$$

$$\lim_{r\to\infty}\sqrt{r}\left(\frac{\partial\widetilde{\mathbf{u}}^{sct}_{\beta}(r)}{\partial r}-ik_{\beta}\,\widetilde{\mathbf{u}}^{sct}_{\beta}(\mathbf{r})\right)=\widetilde{\mathbf{0}},\quad\beta=p,s,\tag{51}$$

for $\mathbf{y}_o \in D \cap \mathcal{G}$. *Simultaneously, denote by* $\widetilde{\breve{\mathbf{u}}}^{sct}_{\mathbf{y}_o}(\mathbf{r})$ *the unique solution of the mixed impedance transmission problem* (46)–(51)*, but this time replacing* $\mathrm{B} \setminus \overline{\mathrm{D}}_1$ *and* D_1 *by* $B \setminus \overline{\breve{D}}_1$ *and* $\breve{D}_1$*, respectively. Then*

$$\widetilde{\mathbf{u}}^{sct}_{\mathbf{y}_o}(\mathbf{r}) = \widetilde{\breve{\mathbf{u}}}^{sct}_{\mathbf{y}_o}(\mathbf{r}), \quad \mathbf{r} \in \overline{\mathcal{G}}. \tag{52}$$

***Proof*:** Taking into account (45) and using Rellich's lemma [32], we obtain $\widetilde{\mathbf{u}}^{\mathrm{sct}}(\mathbf{r}, \hat{\mathbf{d}}) = \widetilde{\breve{\mathbf{u}}}^{\mathrm{sct}}(\mathbf{r}, \hat{\mathbf{d}})$ and $T\widetilde{\mathbf{u}}^{\mathrm{sct}}(\mathbf{r}, \hat{\mathbf{d}}) = \mathrm{T}\widetilde{\breve{\mathbf{u}}}^{\mathrm{sct}}(\mathbf{r}, \hat{\mathbf{d}})$, for $\mathbf{r} \in \partial B$. Holmgren's principle [33] via the latter relations, yield

$$\widetilde{\mathbf{u}}^{\mathrm{sct}}_{\mathbf{y}_o}(\hat{\mathbf{d}}) = \widetilde{\breve{\mathbf{u}}}^{\mathrm{sct}}_{\mathbf{y}_o}(\hat{\mathbf{d}}), \quad \text{with } \mathbf{y}_o \in D \cap \mathcal{G}. \tag{53}$$

Combining the mixed reciprocity relation (34) and (53) we have $\widetilde{\mathbf{u}}_{\infty,y_0}(\hat{\mathbf{d}}) = \widetilde{\breve{\mathbf{u}}}_{\infty,y_0}(\hat{\mathbf{d}})$, for all $\hat{\mathbf{d}} \in S_1$. From Rellich's lemma, the latter relations imply $\widetilde{\mathbf{u}}^{\mathrm{sct}}_{y_0}(\mathbf{r}) = \widetilde{\breve{\mathbf{u}}}^{\mathrm{sct}}_{y_0}(\mathbf{r})$ as well as $\mathrm{T}\widetilde{\mathbf{u}}^{\mathrm{sct}}_{y_0}(\mathbf{r}) = \mathrm{T}\widetilde{\breve{\mathbf{u}}}^{\mathrm{sct}}_{y_0}(\mathbf{r})$, $\mathbf{y}_o \in D \cap \mathcal{G}$. Using again Holmgren's uniqueness theorem the assertion of the theorem follows. □

The unique solution mentioned in Theorem 2.2 of the scattering problem (46)–(51) is secured by the well-posedness of the boundary value problem (24)–(29), details can be found in [12]. In the sequel, and taking into account the mixed reciprocity principle of Theorem 2.1, with the aid of Theorem 2.2 we have the following uniqueness result. Its proof is omitted for brevity and details with a more analytical study can be found in [34] which is communicated separately.

Theorem 2.5: *Assume that* D_1 *and* $\breve{D}_1$ *are two scattering rigid bodies or two scattering non-penetrable partially coated obstacles embedded in the same elastic piecewise-constant background medium* $B \subset \mathbb{R}^2$ *with* $c > 0$, $\breve{c} > 0$ *the corresponding surface impedance constants. If the far-field patterns of the scattered fields for the same incident plane-wave coincide at a fixed frequency, for all incident direction* $\hat{\mathbf{d}} \in S_1$*, and observation direction* $\hat{\mathbf{r}} \in S_1$*, then*

(i) *for the rigid body case*

$$D_1 = \breve{D}_1 \quad \textit{and} \quad \Gamma = \breve{\Gamma}, \tag{54}$$

and

(ii) *for the partially coated case*

$$\Gamma_D = \breve{\Gamma}_D, \qquad \Gamma_I = \breve{\Gamma}_I, \qquad c = \breve{c}. \tag{55}$$

3. The $(F^*F)^{1/4}$-method and its linchpin with the inversion scheme

In this section and for the sake of reader's convenience, we will review basic ideas for finding approximations of the solution to the inverse elastic scattering Dirichlet problem. In particular, we will review the *factorization method* involving full far-field patterns, which are used successfully for the reconstruction of boundaries of scatterers treated in a large variety of inverse acoustic, electromagnetic and elastic problems [1,2,35]. In this paper, we will apply this method to inverse elastic scattering problems, and we will deal with reconstructions of the boundary ∂D of a rigid obstacle for which a homogeneous Dirichlet boundary condition is considered.

Adaptation of this sampling method in inverse elastic scattering problems [36], is to determine a density $\mathbf{g}(\cdot, \mathbf{y}_o;\ \mathbf{p}) = \big(g_p(\cdot, \mathbf{y}_o;\ \mathbf{p}), g_s(\cdot, \mathbf{y}_o;\ \mathbf{p})\big)$ that solves the far-field equation

$$(F^*F)^{1/4}\mathbf{g}(\cdot, \mathbf{y}_o;\ \mathbf{p}) = \mathbf{\Gamma}^{\infty}(\cdot, \mathbf{y}_o;\ \mathbf{p}) \tag{56}$$

with $\mathbf{p} \in S_1$ being the polarization vector of an elastic point-source (see (16)), and $\mathbf{\Gamma}^{\infty}(\cdot, \mathbf{y}_o; \mathbf{p})$ is the far-field pattern of $\mathbf{\Gamma}(\mathbf{r}, \mathbf{y}_o; \mathbf{p})$ given in (17)–(19). Similar to the *linear sampling method* (LSM) [3], the L^2-norm of the solution $\mathbf{g}$ of (56) characterizes the support of the scatterer, with F^* being the Hilbert adjoint operator of F. From the knowledge of the density $\mathbf{g}(\cdot, \mathbf{y}_o;\ \mathbf{p}) \in L^2(S_1)$, the boundary of our obstacle can be recovered at the points where the L^2-norm of the solution has an extremely large value, or equivalently, is not bounded.

At this point and in order to understand the notions in the far-field Equation (56), we introduce the incident field

$$\begin{aligned}\mathbf{v}_g^{\text{inc}}(\mathbf{r}) = e^{-i\pi/4}\Bigg[&\int_{S_1}\sqrt{\frac{k_p}{\omega}}\, g_p(\hat{\mathbf{d}}, \mathbf{y}_o;\ \mathbf{p})\,\hat{\mathbf{d}}\; e^{ik_p\mathbf{r}\cdot\hat{\mathbf{d}}}\,ds(\hat{\mathbf{d}})\\ &+\int_{S_1}\sqrt{\frac{k_s}{\omega}}\, g_s(\hat{\mathbf{d}}, \mathbf{y}_o;\ \mathbf{p})\,\hat{\mathbf{d}}^{\perp}\, e^{ik_s\mathbf{r}\cdot\hat{\mathbf{d}}}\,ds(\hat{\mathbf{d}})\Bigg].\end{aligned} \tag{57}$$

The above relation refers to a superposition of plane waves over the unit circle S_1 propagating in every direction, and the components $g_p(\hat{\mathbf{d}}, \mathbf{y}_o;\ \mathbf{p})$, $g_s(\hat{\mathbf{d}}, \mathbf{y}_o;\ \mathbf{p})$ are known as the longitudinal and transverse Herglotz kernels [24,37]. The far-field patterns of the scattered fields corresponding to the incident wave field (57) are expressed via the elastic far-field operator $F : [L^2(S_1)]^2 \to [L^2(S_1)]^2$ given by

$$\begin{aligned}(F\mathbf{g})(\hat{\mathbf{r}}) = e^{-i\pi/4}\Bigg[&\int_{S_1}\sqrt{\frac{k_p}{\omega}}\,\mathbf{u}^{\infty}(\hat{\mathbf{r}}, \hat{\mathbf{d}}, \hat{\mathbf{d}})\, g_p(\hat{\mathbf{d}}, \mathbf{y}_o;\ \mathbf{p})\,ds(\hat{\mathbf{d}})\\ &+\int_{S_1}\sqrt{\frac{k_s}{\omega}}\,\mathbf{u}^{\infty}(\hat{\mathbf{r}}, \hat{\mathbf{d}}, \hat{\mathbf{d}}^{\perp})\, g_s(\hat{\mathbf{d}}, \mathbf{y}_o;\ \mathbf{p})\,ds(\hat{\mathbf{d}})\Bigg]\end{aligned} \tag{58}$$

where $e^{-i\pi/4}\sqrt{\frac{k_\alpha}{\omega}}\, g_\alpha$, $\alpha = p, s$ are the $L^2(S_1)$-kernels, and $\hat{\mathbf{r}}, \hat{\mathbf{d}}$ denote the observation and incident directions, respectively. Concerning the far-field patterns $\mathbf{u}^{\infty}$, we have the following notation

$$\mathbf{u}^{\infty}(\cdot, \hat{\mathbf{d}}, \hat{\mathbf{d}}) = (u^{\infty,p}(\cdot, \hat{\mathbf{d}}, \hat{\mathbf{d}}),\ u^{\infty,s}(\cdot, \hat{\mathbf{d}}, \hat{\mathbf{d}})) \tag{59}$$

$$\mathbf{u}^{\infty}(\cdot, \hat{\mathbf{d}}, \hat{\mathbf{d}}^{\perp}) = (u^{\infty,p}(\cdot, \hat{\mathbf{d}}, \hat{\mathbf{d}}^{\perp}),\ u^{\infty,s}(\cdot, \hat{\mathbf{d}}, \hat{\mathbf{d}}^{\perp})). \tag{60}$$

Basic known properties of the elastic far-field operator F hold [17,18,36,38]. In particular the far-field operator F is normal, compact and injective. Indeed, since $F : [L^2(S_1)]^2 \to [L^2(S_1)]^2$ is an integral operator with weakly singular kernel, compactness of F is secured. Concerning now injectivity, we have to deal with the existence of the so-called Dirichlet eigenvalue of the operator $-\Delta^*$ in the interior of the scatterer D, whereas for the normality of F, see details in [36] for the Dirichlet case, and in [18] for the transmission case (Theorem 2, p.724).

We move on with our analysis, by defining the auxiliary elastic Herglotz wave operator $H : [L^2(S_1)]^2 \to [H^{1/2}(\partial D)]^2$ as [13]

$$(H\mathbf{g})(\mathbf{r}) := e^{-i\pi/4} \int_{S_1} \left[\sqrt{\frac{k_p}{\omega}}\, \mathbf{g}_p(\hat{\mathbf{d}})\, e^{ik_p \mathbf{r}\cdot\hat{\mathbf{d}}} + \sqrt{\frac{k_s}{\omega}}\, \mathbf{g}_s(\hat{\mathbf{d}})\, e^{ik_s \mathbf{r}\cdot\hat{\mathbf{d}}} \right] ds(\hat{\mathbf{d}}), \tag{61}$$

for $\mathbf{r} \in \partial D$ (recall here that $H\mathbf{g}$ is an entire solution of the Navier equation $\Delta^* \nu + \rho\omega^2 \nu = \mathbf{0}$, in $\mathbb{R}^2 \setminus \overline{D}$. Hence, the adjoint $H^* : [H^{-1/2}(\partial D)]^2 \to [L^2(S_1)]^2$ of operator (61) is given by

$$(H^*\phi)(\hat{\mathbf{r}}) := e^{\frac{i\pi}{4}} \int_{\partial D} \left[\sqrt{\frac{\omega}{k_p}}\, \phi_p(\mathbf{r}')\, e^{-ik_p \mathbf{r}'\cdot\hat{\mathbf{r}}} + \sqrt{\frac{\omega}{k_s}}\, \phi_s(\mathbf{r}')\, e^{-ik_s \mathbf{r}'\cdot\hat{\mathbf{r}}} \right] ds(\mathbf{r}'), \tag{62}$$

where $\hat{\mathbf{r}} \in S_1$, and one can easily see that (62) is the far-field pattern of the weak solution

$$\mathbf{l}(\mathbf{r}) = \int_{\partial D} \widetilde{\Gamma}(\mathbf{r}, \mathbf{r}')\ \phi(\mathbf{r}')\, ds(\mathbf{r}'), \tag{63}$$

of the Dirichlet problem. In the latter relation $\widetilde{\Gamma}(\mathbf{r}, \mathbf{r}')$ is the Green's function corresponding to the Navier equation, since now we have taken into account the boundary value problem (7)–(9). Recall here that the far-field pattern $\mathbf{\Gamma}^\infty(\hat{\mathbf{r}}, \mathbf{y}_0; \mathbf{p}) = \left(\Gamma^{\infty,p}(\hat{\mathbf{r}}, \mathbf{y}_0; \mathbf{p}),\ \Gamma^{\infty,s}(\hat{\mathbf{r}}, \mathbf{y}_0; \mathbf{p}) \right)$ of $\mathbf{\Gamma}(\mathbf{r}, \mathbf{y}_0; \mathbf{p})$ is given by (18) and (19). We also define the operator $\mathcal{A} : [H^{1/2}(\partial D)]^2 \to [L^2(S_1)]^2$ which maps an $\mathbf{h} \in [H^{1/2}(\partial D)]^2$ into the far-field pattern of the radiating weak solution $\mathbf{l}$ (see (63)), of the Dirichlet problem, i.e. $\mathcal{A}\mathbf{h} = \mathbf{l}_\infty$ with $\mathbf{l} = \mathbf{h}$ on the boundary ∂D. The definition now of operator $\mathcal{A}$ implies that

$$\mathcal{A}(\mathbf{l}|_{\partial D}) = H^*(\phi) \tag{64}$$

with $\mathcal{A}(\mathbf{l}|_{\partial D}) \equiv \mathcal{A}(S\phi)$, where $S : [H^{-1/2}(\partial D)]^2 \to [H^{1/2}(\partial D)]^2$ is given by

$$(S\phi)(\mathbf{r}) = \int_{\partial D} \widetilde{\Gamma}(\mathbf{r}, \mathbf{r}')\ \phi(\mathbf{r}')\, ds(\mathbf{r}'), \quad \mathbf{r} \in \partial D. \tag{65}$$

We also observe that $F\mathbf{g}$ is the far-field pattern of the solution to the Dirichlet problem corresponding to the incident field $-H\mathbf{g}(\mathbf{r})$, $\mathbf{r} \in D$, and hence

$$F = -\mathcal{A}H \tag{66}$$

Via relations (64) and (66) we easily obtain the factorization

$$F = -\mathcal{A}S^*\mathcal{A}^*. \tag{67}$$

Extended analysis for the later relation, concerning the elastic Dirichlet and transmission problem, can be found in [36] and [13], respectively. Considering the above analysis, recalling the definition of operator $\mathcal{A}$, and taking into account the singular system of the operator F we have the result [2]: *If we assume that ω^2 is not an interior Dirichlet eigenvalue in D, then*

$$Range(\mathcal{A}) = Range\left((F^\star F)^{1/4} \right). \tag{68}$$

Further it has been also proved [36] that: *if we assume that D is simply connected and ω^2 is not an interior Dirichlet eigenvalue in D, then for any $\mathbf{y}_0 \in \mathbb{R}^2$, the function*

$$\mathbf{\Gamma}^{\infty}(\hat{\mathbf{r}}, \mathbf{y}_0; \mathbf{p}) \in Range(\mathcal{A}) \iff \mathbf{y}_0 \in D. \tag{69}$$

The latter is concerned with the simple characterization of the support of the elastic scatterer D. Therefore, we adapted the factorization method for inverse scattering by an elastic rigid body concerning the case of full far-field patterns. A modified factorization method was proposed in [31], where shape reconstructions using only one part (P or S-part) of the far-field pattern were given, as well as they provided uniqueness results [31] (Theorems 3.7 and 3.8) by considering only one type of elastic plane waves. Extra uniqueness results on inverse elastic scattering problems can also be found in [39,40].

In what follows numerical results for two-dimensional elastic obstacles will be given. We apply a new numerical technique (IMPC) under the framework of the factorization method, in order to recover the shape of an elastic (rigid) body considering: full far-field patterns, and P or S-part of the far-field patterns. Via IMPC we give various numerical examples which illustrate the accuracy of our 2D shape reconstructions.

4. Numerical examples

For N longitudinal (pressure) waves or N transverse (shear) waves, incident from N directions $\hat{\mathbf{d}}_j = (cos\theta_j, \sin\theta_j)$ with $\theta_j = 2\pi j/N$, we assume that the far-field equation (56) is discretized as described in [31], giving rise to a system of $2N \times 2N$ linear equations

$$(\widetilde{F}^{*}\widetilde{F})^{1/4} g_{\mathrm{y_o}} = b^{(\mathrm{y_o})}, \qquad \widetilde{F} \in C^{2N\times 2N}, \tag{70}$$

where $b^{(\mathrm{y_o})}$ is a discrete version of $\Gamma^{\infty}_{\mathrm{y_o}}$ and $\widetilde{F}$ is a discretized version of the far-field operator F. We shall consider the reconstruction problem in three cases:

(i) *FF* case based on the operator F (full far-field pattern),
(ii) *PP* case based on the operator F_p (part of the far-field pattern corresponding to N incident plane longitudinal waves), and
(iii) *SS* case based on the operator F_s (part of the far-field pattern corresponding to N incident plane transverse waves).

A discretized version of F_p (resp. F_s) denoted by $\widetilde{F}_p$ (resp. $\widetilde{F}_s$) can be extracted from $\widetilde{F}$ by taking rows 1 (resp. $N+1$) through N (resp. $2N$) and columns 1 (resp. $N+1$) through N (resp. $2N$).

In all cases, for some chosen polarization vector and for each sampling point $\mathbf{y}_{\mathrm{o}} \in \mathbb{R}^2$, the profile of the object can be recovered by plotting the indicator function

$$W(\mathbf{y}_o) = \left[\sum_{j=1}^{M} \frac{|\alpha_j|^2}{\eta_j} \right] \tag{71}$$

where $M = 2N$ in the *FF* case or $M = N$ in the other cases, α_j is the component of $b^{(\mathrm{y_o})}$ along the j-th right singular vector of $\widetilde{F}$ in the *FF* case, or the component of $b^{(\mathrm{y_o},p)}$ (resp. $b^{(\mathrm{y_o},s)}$) along the j-th right singular vector of $\widetilde{F}_p$ in the other case (resp. $\widetilde{F}_s$), and η_j is the

corresponding singular value. Here, $b^{(\mathrm{y_o},p)}$ (respectively, $b^{(\mathrm{y_o},s)}$) denotes the vector of N first (resp. last) components of $b^{(\mathrm{y_o})}$.

However, since the noisy data case is not covered in (71), our main purpose is to deal with the reconstruction problem using noisy far-field data,

$$\widetilde{F}_\epsilon = \widetilde{F} + \epsilon \|\widetilde{F}\| \mathcal{N}, \tag{72}$$

where $\widetilde{F}_\epsilon$ is the noisy counterpart of the matrix $\widetilde{F}$, $\mathcal{N}$ is a random noise matrix normalized such that $\|\mathcal{N}\| = 1$ and ϵ is an error parameter which determines the amount of noise in the data. Thus, the results described below may be regarded as a complement of what is described in [31] where only unregularized reconstructions are reported. Our strategy is to consider a version of (71) based on Tikhonov regularization where the regularization parameter is chosen by the generalized discrepancy principle (GDP) and the IMPC [4]. The regularized counterpart of (71) corresponding to the FF case becomes

$$W(\mathrm{y_o}, \lambda) = \left[\sum_{j=1}^{M} \frac{\eta_j |\alpha_j|^2}{(\lambda^2 + \eta_j)^2} \right] \tag{73}$$

which is nothing more than the reciprocal of $\|g_{\lambda,\mathrm{y_o}}\|^2$, where $g_{\lambda,\mathrm{y_o}}$ is defined as

$$g_{\lambda,\mathrm{y_o}} = \underset{g \in C^N}{\operatorname{argmin}} \{ \|\widetilde{A}\, g - b^{(\mathrm{y_o})}\|_2^2 + \lambda^2 \|g\|_2^2 \}, \tag{74}$$

where λ is the regularization parameter and $\widetilde{A} = (\widetilde{F}_\epsilon^* \widetilde{F}_\epsilon)^{1/4}$. Indicator functions associated to the *PP* and *SS* cases are defined similarly.

4.1. On GDP and IMPC

For efficiency, GDP and IMPC are implemented following the fast fixed point iteration approaches from [6,41]. Recall that GDP chooses as regularization parameter the only root of the nonlinear equation

$$G(\lambda) = \|\widetilde{A}\, g_{\lambda,\mathrm{y_o}} - b^{(\mathrm{y_o})}\|_2^2 - \delta_{\mathrm{A}}^2 \, \|g_{\lambda,\mathrm{y_o}}\|_2^2 = 0 \tag{75}$$

where δ_{A} is an estimate for $\|E\| = \|\widetilde{A} - A\|$ such that $\|E\| \le \delta_{\mathrm{A}}$.

It is well known that G is convex for small λ and concave for large λ. As a result, global and monotone convergence of Newton's method cannot be guaranteed [42]. This difficulty is circumvented by the GDP-FP algorithm introduced by Bazán [41], as we will see shortly.

Let us now consider

$$\mathsf{r}(\lambda) = \|\widetilde{A}\, g_{\lambda,\mathrm{y_o}} - b^{(\mathrm{y_o})}\| \ \text{ and } \ \mathsf{s}(\lambda) = \|g_{\lambda,\mathrm{y_o}}\|, \tag{76}$$

and for $\lambda_0 > 0$ we define the sequence

$$\lambda_{\mathrm{k}+1} := \xi(\lambda_{\mathrm{k}}), \ k = 0, 1, 2, \ldots, \quad \xi(\lambda) = \lambda \sqrt{\frac{\delta_{\mathrm{A}}\, \mathsf{s}(\lambda)}{\mathsf{r}(\lambda)}}. \tag{77}$$

Bazán [41] showed that the sequence above converges globally to the unique root of $G(\lambda)$ irrespective of the chosen initial guess. Thus, provided the solution norm and the corresponding residual norm are available, computing the regularization parameter chosen by GDP is easy. A difficulty with GDP is that it requires knowledge of the noise level δ_{A}: poor quality solutions may be produced when the noise level is not accurately estimated.

An alternative parameter selection criterion that avoids knowledge of the noise level and that have been shown to produce excellent 2D reconstructions is the MPC [4]. MPC selects as regularization parameter a maximum point of the function

$$\Psi(\lambda) = \left[\mathsf{r}(\lambda)\right]^2 \left[\mathsf{s}(\lambda)\right]^2 \tag{78}$$

which is relatively simple to compute in most cases. However, MPC is not free of difficulties and can fail when Ψ has several local maxima. IMPC circumvents this by selecting the regularization parameter as the largest maximum point of Ψ and by introducing a fixed point procedure for its computation. Thus, algorithmically, the regularization parameter chosen by IMPC is computed as the limit value of the sequence

$$\lambda_{k+1} = \chi(\lambda_k), \ k = 0, 1, 2, \ldots, \quad \chi(\lambda) = \frac{\lambda^2\, \mathsf{s}(\lambda)}{\mathsf{r}(\lambda)} \tag{79}$$

under the assumption that the initial guess is chosen in the interval $\left[\frac{\sqrt{3}}{3}\sqrt{\eta_1},\ \sqrt{\eta_1}\right]$ (see [6], Theorem 3.2).

We emphasize that both fixed point approaches (77) and (79) require computing the regularized solution norm $\mathsf{s}(\lambda)$ and the corresponding residual norm $\mathsf{r}(\lambda)$ and that both of them can be efficiently implemented by using the SVD of the far-field matrix $\widetilde{F}_\epsilon$. In practice, the calculation of approximations λ_j should stop when they begin to stagnate in order to keep small the computational cost of the entire process. In our implementation we choose to stop the iterations when the relative change of consecutive values is small, i.e. when

$$|\lambda_{k+1} - \lambda_k| \leq \nu\, |\lambda_k|, \tag{80}$$

where ν is a small tolerance parameter.

4.2. On the reconstruction

We now describe some reconstruction results corresponding to the three objects shown in Figure 3, namely a kite-shaped object, an acorn-shaped object, and a peanut-shaped object.

For the numerical reconstructions we consider a uniform grid in the square $[-2,\ 2\,] \times [-2,\ 2\,]$ containing the object, with 100 points in each direction, and use noisy far-field matrices of order 128×128, choosing error parameters $\epsilon = 0.01$ (relative noise level 1%) and $\epsilon = 0.1$ (relative noise level 10%), see Equation (72). The synthetic 'noise-free' far-field data used in the experiments are generated as in [31] using parametric forms of the integrals that represent the *P*-part and *S*-part of the scattered field. Reconstruction results based on exact far-field data obtained by plotting the indicator function (71), are displayed in Figure 1. Note that, in general, the reconstructions corresponding to the *FF* case are of superior quality when compared with those of the other cases. The reason is that, in general, the far-field matrix associated to the *FF* case is less sensitive to noise than the

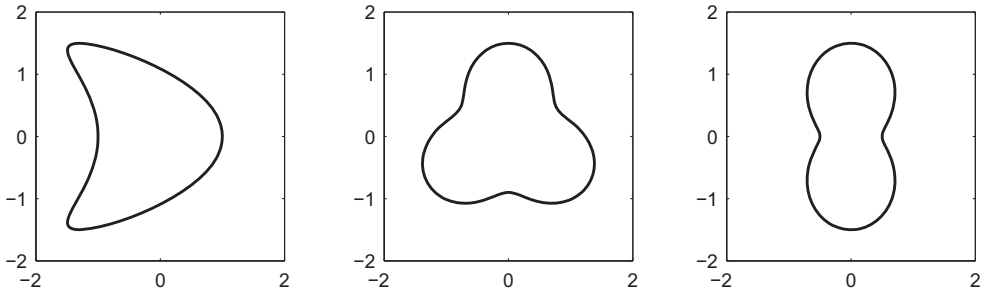

Figure 3. Objects to be reconstructed.

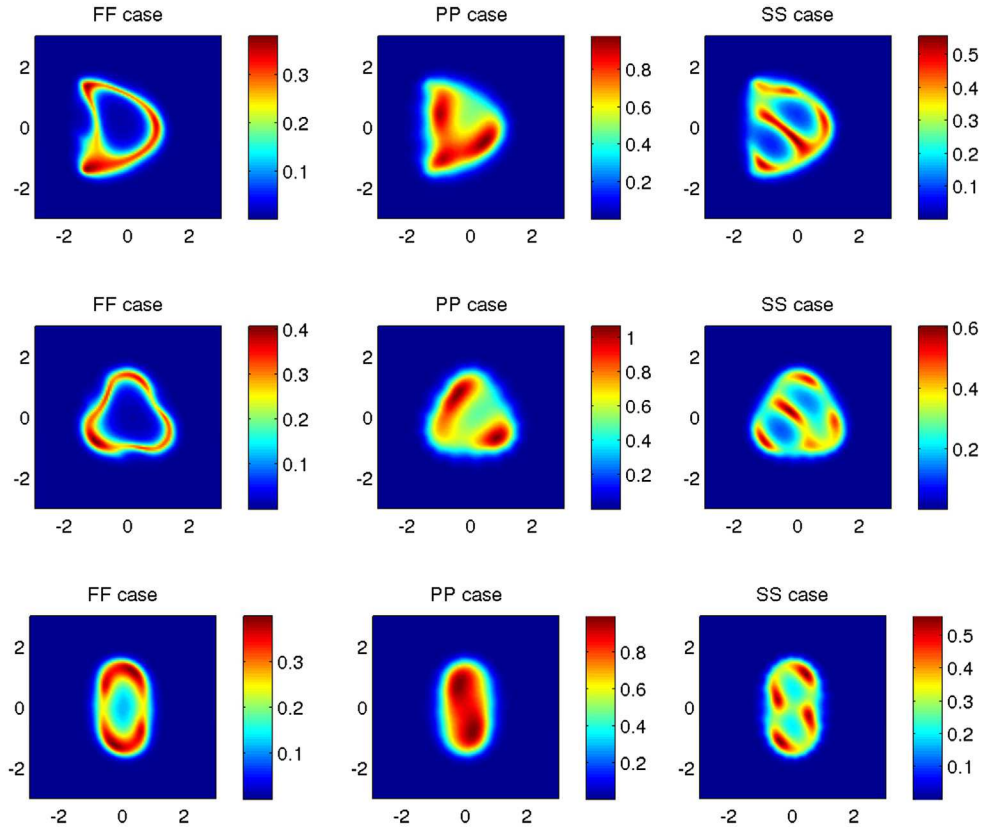

Figure 4. Reconstruction results for 3 objects using exact far-field data.

matrices associated to other cases. For illustration, for the peanut-shaped object we have $cond(F) = 2.7173 \times 10^{10}, cond(F_p) = 3.0767 \times 10^{10}$ and $cond(F_s) = 9.3502 \times 10^{15}$.

In our implementation of GDP-FP and IMPC we use the SVD of $\widetilde{F}_\epsilon$ and for the tolerance parameter in (80) we choose $\nu = 10^{-4}$. The first point worth mentioning is that in all numerical examples, the number of iterations spent until the stopping criterion is reached never exceeded $k = 12$ for GDP-FP and $k = 17$ for IMPC. This not only verifies the excellent performance of GDP-FP when applied to other problems, see [41], but also shows

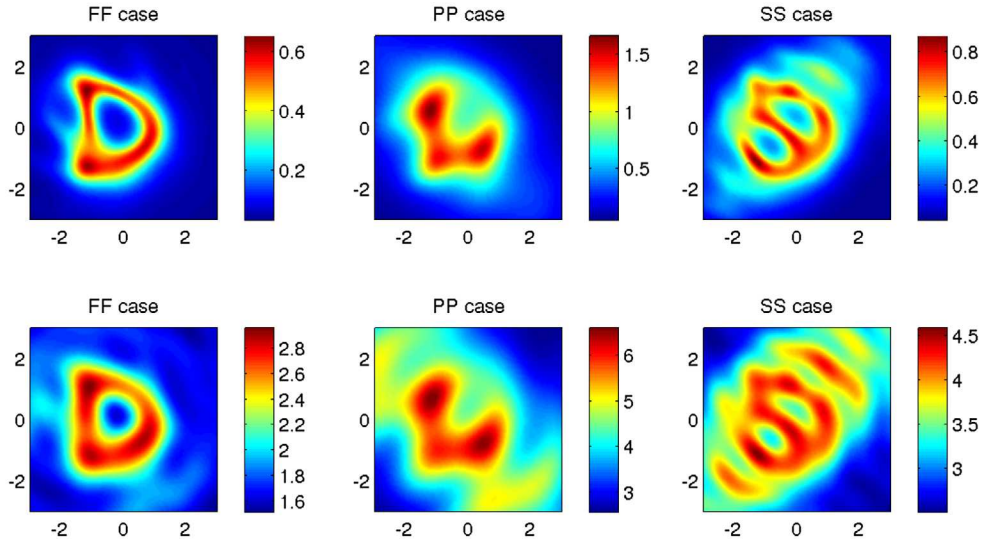

Figure 5. Reconstruction results for kite-shaped object obtained with GDP. Noise level 1% (top) and 10% (bottom).

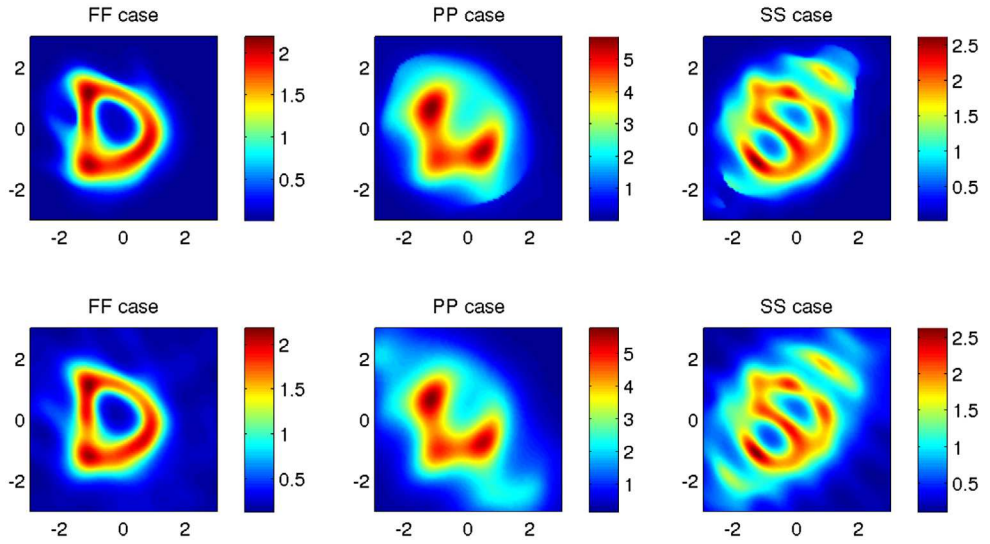

Figure 6. Reconstruction results for kite-shaped object obtained with IMPC. Noise level 1% (top) and 10% (bottom).

that it can be an effective tool in conjunction with linear sampling in inverse scattering problems. The reconstructions of the kite-shaped object obtained with GDP-FP for the three cases are displayed in Figure 5, while the reconstructions obtained with IMPC are displayed in Figure 6.

As we can observe, both approaches identify the presence and shape of the object still when the data is highly contaminated by noise, but with a remarkable advantage in favour of the *FF* case. This was expected however, since the *FF* case carries more data and hence

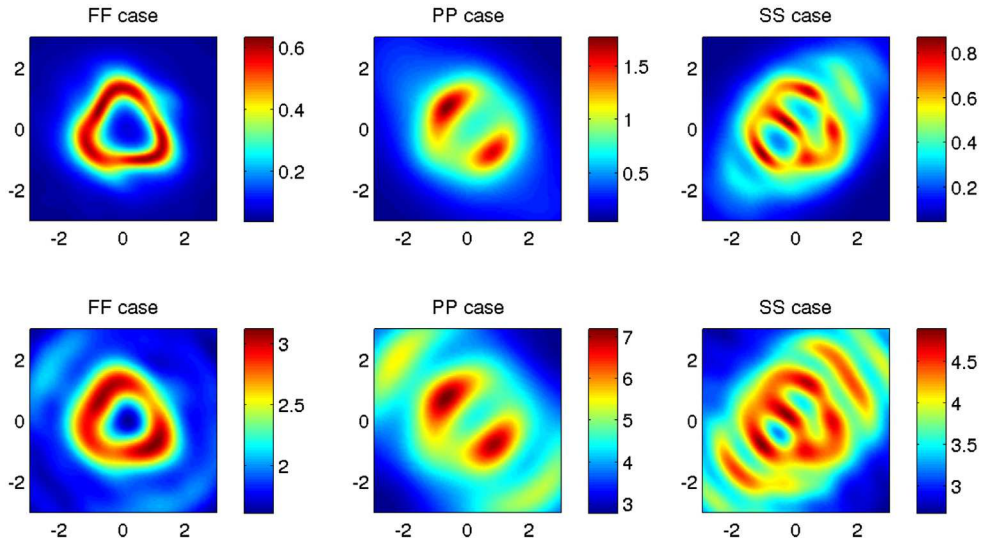

Figure 7. Reconstruction results for acorn-shaped object obtained with GDP. Noise level 1% (top) and 10% (bottom).

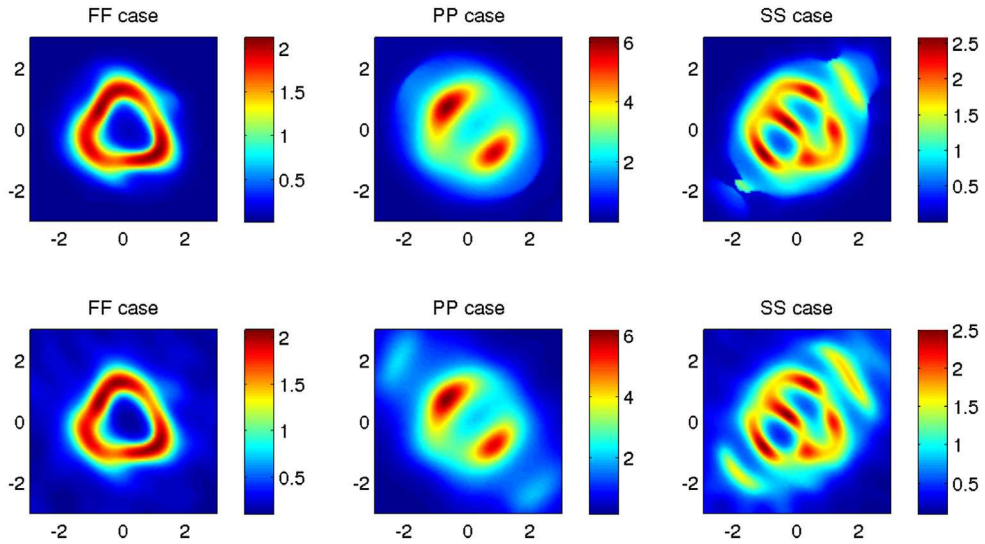

Figure 8. Reconstruction results for acorn-shaped object obtained with IMPC. Noise level 1% (top) and 10% (bottom).

more information about the scatterer. It is well known that the LSM requires a large number of data to yield reliable reconstructions.

Reconstruction results for the acorn-shaped object shown in Figures 7 and 8 show a similar trend: while the reconstructions in the *FF* case look fine, the same does not occur with the reconstruction in the *PP* and *SS* cases which show poor quality. As it is also mentioned in [31], a possible explanation is that the *S*-part and *P*-part of the scattered field alone exhibit stronger singularities compared to the *FF* case where they are combined.

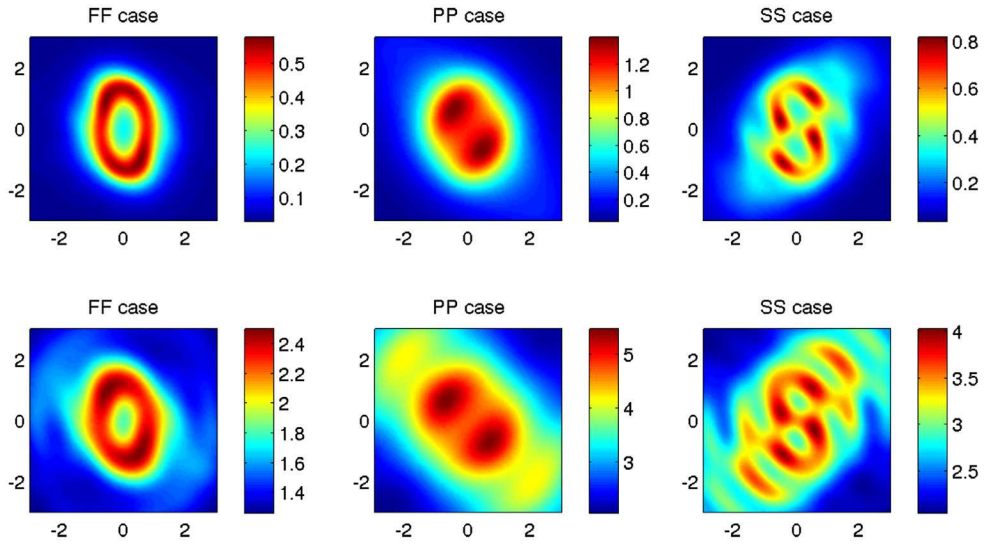

Figure 9. Reconstruction results for peanut-shaped object obtained with GDP. Noise level 1% (top) and 10% (bottom).

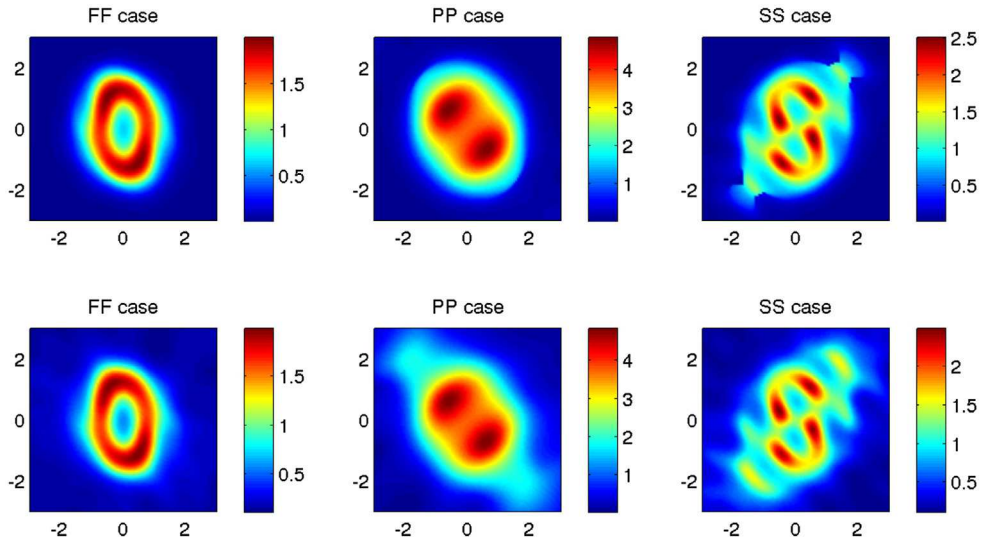

Figure 10. Reconstruction results for peanut-shaped object obtained with IMPC. Noise level 1% (top) and 10% (bottom).

Finally, reconstruction results of the peanut-shaped object are displayed in Figures 9 and 10. Again we see that the quality of the reconstructions obtained in the case *FF* exceeds the quality of those obtained in the *PP* and *SS* cases.

5. Conclusions-remarks

The paper at hand establishes new results concerning a numerical reconstruction method in inverse scattering by elastic obstacles. Due to elastic plane waves (see (3)), the direct and inverse scattering problem were introduced in order to present uniqueness results, as well as to present an inversion algorithm concerning shape reconstructions via the new numerical technique IMPC. We also make the following remarks:

(i) From the theoretical point of view, the general case of mixed boundary conditions corresponding to the so-called *partially coated obstacle* were considered. Our inverse elastic scattering problem was described by the mixed impedance transmission boundary value problem (24)–(28), and uniqueness results which are valid for the Dirichlet case as well, were established.

(ii) Concerning our numerical treatment, incident elastic plane waves of the form (3) were used. Our numerical reconstruction method also holds if only one type of incident elastic plane wave (*P* or *S*-wave) occurs. In addition numerical experiments were given, showing satisfactory results by using the *P*-part or *S*-part of the far-field pattern. Further, a discussion concerning reconstruction and comparing issues among the *FF*, *PP* and *SS* case were also given.

Disclosure statement

No potential conflict of interest was reported by the authors.

References

[1] Kirsch A. Characterization of the shape of the scattering obstacle by the spectral data of the far-field operator. Inverse Prob. 1998;14:1489–1512.
[2] Kirsch A, Grinberg N. The factorization method for inverse problems. Vol. 36, Oxford lecture series in mathematics and its applications. Oxford: Oxford University Press; 2008.
[3] Colton D, Kirsch A. A simple method for solving the inverse scattering problems in the resonance region. Inverse Prob. 1996;12:383–393.
[4] Bazán FSV, Francisco JB, Leem KH, et al. A maximum product criterion as a Tikhonov parameter choice rule for Kirsch's factorization method. J Comput Appl Math. 2012;236:4264–4275.
[5] Colton D, Pianna M, Potthast R. A simple method using Morozov's discrepancy principle for solving inverse scattering problems. Inverse Prob. 1999;13:1477–1493.
[6] Bazán FSV, Francisco JB, Leem KH, et al. Using the Linear Sampling method and an improved maximum product criterion for the solution of the electromagnetic inverse medium problem. J Comput Appl Math. 2015;273:61–75.
[7] Bazán FSV, Kleefeld A, Leem KH, Pelekanos G. Sampling method based projection approach for the reconstruction of 3D acoustic penetrable scatterers. Linear Algebra Appl. 2016;495:289–323.
[8] Twersky V. Multiple scattering of electromagnetic waves by arbitrary configurations. J Math Phys. 1967;8:589–610.
[9] Tai CT. Dyadic greens functions in electromagnetic theory. New York (NY): IEEE; 1994.
[10] Kupradze VD, Gegelia TG, Basheleishvili MO, et al. Three dimensional problems of the mathematical theory of elasticity and thermoelasticity. North Holland series in applied mathematics and mechanics. Amsterdam: North Holland Publishing Company; 1979.

[11] Natrosvilli D, Tediashvili Z. Mixed type direct and inverse scattering problems. In: Elschner J, Gohberg I , Silbermann B . editors. Problems and methods in mathematical physics. Vol. 121, Operator theory: advances and applications. Basel: Birkhäuser; 2001. p. 366–389.
[12] Athanasiadis CE, Natroshvili D, Sevroglou V, et al. A boundary integral equations approach for mixed impedance problems in elasticity. J Integral Equ Appl. 2011;23:183–222.
[13] Pelekanos G, Sevroglou V. The $(F^*F)^{1/4}$-method for the transmission problem in two-dimensional linear elasticity. Appl Anal. 2005;84:311–328.
[14] Sevroglou V, Pelekanos G. An inversion algorithm in two-dimensional elasticity. J Math Anal Appl. 2001;263:277–293.
[15] Athanasiadis CE, Natroshvili D, Sevroglou V, et al. An application of the reciprocity gap functional to inverse mixed impedance problems in elasticity. Inverse Prob. 2010;26:085011, 19pp.
[16] Athanasiadis CE, Sevroglou V, Stratis IG. Scattering relations for point generated dyadic fields in two-dimensional linear elasticity. Q Appl Math. 2006;64:695–710.
[17] Pelekanos G, Sevroglou V. Inverse scattering by penetrable objects in two-dimensional elastodynamics. J Comput Appl Math. 2003;151:129–140.
[18] Sevroglou V. The far-field operator for penetrable and absorbing obstacles in 2D inverse elastic scattering. Inverse Prob. 2005;17:717–738.
[19] Committee of Coatings for High Temperature Structural Materials. National Materials Advisory Board, Commission of Engineering and Technical Systems National Research Council, Coatings for High Temperature Structural Materials: Trends and Opportunities. Washington, DC: National Academy Press; 1996.
[20] Cherkaoui M, Sabar H, Berveiller M. Micromechanical approach of the coated inclusion problem and applications to composite problems. J Eng Mater Technol. 1994;116:274–278.
[21] Venkatraman S, Tan LP, Joso JF, et al. Biodegradable stents with elastic memory. Biomaterials. 2006;27:1573–1578.
[22] Mu M, Walker AM, Torkelson JM, et al. Cellular structures of carbon nanotubes in a polymer matrix improve properties relative to composites with dispersed nanotubes. Polymer. 2002;49:1332–1337.
[23] 2008. Available from: www.technocarbon.com/fileadmin/Articles/SD_CM_02_08technocarbon.pdf
[24] Dassios G, Kleinmann R. Low-frequency scattering theory. Oxford: Oxford University Press; 1998.
[25] Tanuma K. Stroh formalism and Rayleigh waves. J Elast. 2007;89:5–154.
[26] Athanasiadis CE, Natroshvili D, Sevroglou V, et al. Mixed impedance transmission problems for vibrating layered elastic bodies. Math Meth Appl Sci. 2015;38:3264–3294.
[27] Potthast R. Point sources and multipoles in inverse scattering theory. London: Chapman and Hall/CRC; 2001.
[28] Colton D, Haddar H. An application of the reciprocity gap functional in inverse scattering theory. Inverse Prob. 2005;21:383–398.
[29] Di CM. Sun J. An inverse scattering problem for a partially coated buried obstacle. Inverse Prob. 2006;22:2331–2351.
[30] Athanasiadis CE, Sevroglou V, Stratis IG. 3D elastic scattering theorems for point-generated dyadic fields. Math Meth Appl Sci. 2007;31:987–1003.
[31] Hu G, Kirsch A, Sini M. Some inverse problems arising from scattering rigid obstacles. Inverse Prob. 2013;29:015009, 21pp.
[32] Colton D, Kress R. Inverse acoustic and electromagnetic scattering theory. 2nd ed. Berlin: Springer; 1998.
[33] Kress R. Acoustic scattering: specific theoretical tools. In: Pike R, Sabatier P, editors. Scattering. London: Academic Press; 2001. p. 37–51, 52–73.
[34] Athanasiadis CE, Natroshvili D, Sevroglou V, et al. The inverse problem of elastic scattering by partially coated piecewise homogeneous layered obstacles. 2016. under review.
[35] Charalambopoulos A, Kirsch A, Anagnostopoulos AK, et al. The factorization method in inverse elastic scattering from penetrable bodies. Inverse Prob. 2007;23:27–51.

[36] Alves CJS, Kress R. On the far field operator in elastic obstacle scattering. IMA J Appl Math. 2002;67:1–21.
[37] Sevroglou V, Pelekanos G. Two dimensional elastic Herglotz functions and their applications in inverse scattering. J Elast. 2002;68:123–144.
[38] Arens T. Linear sampling method for 2D inverse elastic wave scattering. Inverse Prob. 2001;17:1445–1464.
[39] Elshner J, Yamamoto M. Uniqueness in inverse elastic scattering with finitely many incident waves. Inverse Prob. 2010;26:045005.
[40] Hahner P, Hsiao G. Uniqueness theorems in inverse obstacle scattering of elastic waves. Inverse Prob. 2010;9:525–534.
[41] Bazán FSV. Simple and efficient determination of the Tikhonov regularization parameter chosen by the generalized discrepancy principle for discrete-ill-posed problems. J Sci Comput. 2015;63:163–184.
[42] Lu S, Pereverzev SV, Shao Y, et al. On the generalized discrepancy principle for Tikhonov regularization in Hilbert scales. J Integral Equ Appl. 2010;22:483–517.